A Classification Scheme for Young Stellar Objects Using the *WIDE-FIELD INFRARED SURVEY EXPLORER AllWISE* Catalog: Revealing Low-Density Star Formation in the Outer Galaxy

X. P. Koenig,[1] D. T. Leisawitz[2]

ABSTRACT

We present an assessment of the performance of *WISE* and the *AllWISE* data release in a section of the Galactic Plane. We lay out an approach to increasing the reliability of point source photometry extracted from the *AllWISE* catalog in Galactic Plane regions using parameters provided in the catalog. We use the resulting catalog to construct a new, revised young star detection and classification scheme combining *WISE* and *2MASS* near and mid-infrared colors and magnitudes and test it in a section of the Outer Milky Way. The clustering properties of the candidate Class I and II stars using a nearest neighbor density calculation and the two-point correlation function suggest that the majority of stars do form in massive star forming regions, and any isolated mode of star formation is at most a small fraction of the total star forming output of the Galaxy. We also show that the isolated component may be very small and could represent the tail end of a single mechanism of star formation in line with models of molecular cloud collapse with supersonic turbulence and not a separate mode all to itself.

Subject headings: circumstellar matter — H II regions — infrared: stars — stars: formation — stars: pre-main-sequence

1. Introduction

The Wide-field Infrared Survey Explorer (*WISE*) mapped the whole sky in 4 mid-infrared bands at 3.4, 4.6, 12, and 22 μm (Wright et al. 2010). The location of these bands in the mid-infrared matches where the excess emission from cooler circumstellar disk/envelope material in young stars begins to become significant in relation to the stellar photosphere.

[1]Yale University

[2]NASA Goddard Space Flight Center, Greenbelt, MD 20771, USA

This fact means that *WISE* can be readily used as a tool to find and classify young stellar objects (YSOs), in a similar way to work carried out with *Spitzer* (Allen et al. 2004, Gutermuth et al. 2008, 2009 and others). However, given its specific set of science goals, the *WISE* pipeline source extraction process was not optimized for the areas where these objects are most commonly found, namely the Galactic Plane. There, YSOs are typically found in regions that are bright in the mid-infrared from thermal dust emission or excited line emission from PAH dust, or regions that are dark as in the case of infrared dark clouds (Rathborne et al. 2006) or in dense clustered regions. These facts necessitate an assessment of *WISE*'s performance in such regions before we set out schemes to achieve our goal of finding YSOs. In a recent paper, Koenig et al. (2012) (hereafter: K12) described a *WISE-2MASS* (Two Micron All Sky Survey, see Skrutskie et al. 2006) YSO identification and classification scheme and applied it to photometry they extracted from their own point source catalogs extracted from custom-made *WISE* mosaic images. While this was practical for a 'pointed' survey such as theirs, a general scheme that can be applied to arbitrarily located and sized portions of the sky is necessary when computational limitations make the construction of huge mosaics prohibitive. An examination of the reliability of the *WISE* catalog in the Galactic Plane should also be generally useful to the science community and is not yet covered in great detail in existing online documentation for the survey.

The properties of the public *WISE* source catalogs stem in part from the choice of source detection run on the four-band imaging data from the telescope. The choice of source detection itself was motivated by the needs of the driving science goals of the mission: to study infrared-bright galaxies, to find brown dwarfs and to study near-Earth asteroids. The online explanatory supplement[1] and Marsh & Jarrett (2012) describe the *WISE* source detection method in detail. The process is based on the thresholding of a 'detection' image derived from a set of matched filter images in the relevant bands. The algorithm calculates an optimal matched filter at each wavelength and combines the resulting single-band images in quadrature to produce a detection image in units of the local standard deviation of noise, and then searches this image for local maxima. It then further deblends candidate point sources by profile-fitting on each individual frame for all bands simultaneously. This process avoids the need for bandmerging and allows for improved detection of sources in the longer wavelength *WISE* bands. However in Galactic star-forming regions it also has the negative consequence of generating detections of the nebular background with apparently good photometric parameters (in particular: signal to noise and photometric uncertainty) in some bands in accompaniment to genuine point source detections in the other bands. In this paper we will document the performance of the *AllWISE* catalog in the Galactic Plane and outline

[1]http://wise2.ipac.caltech.edu/docs/release/allwise/expsup/

approaches to mitigating fake source contamination. We will apply one such approach in order to present a refined version of the YSO classification scheme of K12. This paper will also account in more detail for the various astrophysical sources of contamination that can be misclassified as YSOs by schemes based on infrared colors, for example, Asymptotic Giant Branch (AGB) and Classical Be stars (CBe: rapidly rotating B-type main sequence stars with a geometrically-flattened decretion disk, Rivinius et al. 2013). It should be noted that the *AllWISE* release differs from prior *WISE* releases in how it handles background subtraction and other details of photometric extraction, as described in the explanatory supplement. While the overall approach we lay out in this paper for fake source mitigation and young star identification would be applicable to the Preliminary and All-Sky releases, the precise details would thus differ slightly.

2. Data

In this paper we make use of the *AllWISE* processing of the *WISE* survey data. As part of the online point source catalog, a match to the *2MASS* point-source catalog is automatically included and we include these data as well.

2.1. Properties of *WISE* and the *AllWISE* catalog in the Galactic Plane

In order to understand how *WISE* in general and specifically the *AllWISE* point source extraction perform in Galactic star forming regions, we analyzed two test regions covering parts of the W3 and W5 giant molecular clouds and part of the W4 region (Westerhout 1958). Both the W3/W4 and the W5 test fields encompass on-cloud, bright, nebular emission and off-cloud, lower background regions in their neighboring, ionized H II regions. The W3/W4 field (from here on referred to as just the 'W3' field) additionally incorporates a dark lane or infrared dark cloud. To clarify the following discussion, we adopt lower case italics to refer to the four *WISE* bands, $w1$, $w2$, $w3$ and $w4$ and upper case W3, W4 and W5 to refer to the massive star forming regions.

To estimate the maximum potential completeness of *WISE* in Galactic star forming regions like W3, W4 and W5, we start by constructing a 'truth' catalog for each band for each field from the large *WISE* mosaics of W3, 4 and 5 made by K12 from raw *WISE* frames, since these have slightly higher resolution than the *WISE* atlas tiles available online. This property of the *WISE* image atlas tiles is due to the co-addition process that slightly smoothes these images to optimize them for point source detection, but degrades their angular resolution

by a factor of $\sqrt{2}$ (see the *AllWISE* Explanatory Supplement, section IV.4.l). We search our images for point sources in the test fields by eye, verifying these with reference to the *Spitzer* images of Koenig et al. (2008) for W5 and mosaics from the *Spitzer* Heritage Archive[2] for W3. The *Spitzer* IRAC 3.6 and 4.5 μm and MIPS 24 μm images are a close match to *WISE* bands 1, 2 and 4. The IRAC 8 μm band is not an exact match to *WISE* band 3 at 12 μm, but is close enough in wavelength that point sources bright in these *Spitzer* images are similarly evident in *WISE* 12 μm images, allowing a determination if an apparent *WISE* band 3 point source is in fact a nebular emission knot when seen at the higher sensitivity and resolution of *Spitzer*. In the following discussion we refer to objects in this list and their matched entries in the *WISE* photometric database as 'real' sources, while objects in the database with no match in the truth catalog in a given band are referred to as 'fake' or 'spurious' sources.

Since the point source density varies strongly with waveband, the size of the region surveyed by eye is different between bands. Table 1 lists the test field locations and source sample sizes.

2.2. Completeness of *WISE* and *AllWISE*

The nominal 95% completeness listed for the *WISE* survey in the Explanatory Supplement is appropriate for high Galactic latitude fields with $|b| > 30°$. In magnitudes, the values are: $w1$=17.1, $w2$=15.7, $w3$=11.6 and $w4$=7.7. In the Galactic Plane, as already mentioned, star forming regions contain bright, structured emission from PAH molecules and dust grains excited and heated by radiation from nearby and embedded young stars (Li & Draine 2001) and extinction features like infrared dark clouds. The point source density is also higher in the Galactic Plane and stars are frequently found in dense clusters. As described in Appendix A.1, we determine a measure of the magnitude at which 90% of sources that were detected by *Spitzer* in our test fields are found in the *WISE* images. Table 2 summarizes the results of this calculation. In regions of bright background, the intrinsic detection limit of *WISE* is lower, thus we generate a completeness estimate for regions of high and low sky background in each of our test regions. Because the *WISE* source list was determined by eye with no deblending capability, the true completeness may be slightly better than the quoted values.

The *AllWISE* source extraction pipeline is only able to retrieve a subset of the sources visible in Galactic Plane *WISE* images, because of the issues described earlier. Table 1 lists the number of truth catalog sources found in the *AllWISE* catalog within 2″ (for $w1$ and

[2]http://sha.ipac.caltech.edu/applications/Spitzer/SHA/

Table 1. *WISE* Test Fields and Sample Sizes

Cloud	*WISE* band	Center	Dimensions	N_{SRC}	$N_{non-null}$
W 3	1	2:28:48 +61:32:00.0	17.2×10.6	1713	501
	2	2:28:48 +61:32:00.0	17.2×10.6	1646	488
	3	2:27:30 +61:25:45.0	46×45	704	464
	4	2:26:00 +61:12:20.0	87×96	401	333
W 5	1	2:55:10 +60:40:15.0	14.9×10.65	1633	603
	2	2:55:10 +60:40:15.0	14.9×10.65	1309	583
	3	2:55:00 +60:40:15.0	44.5×44.5	710	549
	4	2:52:50 +60:39:35.0	90×90	399	335

Note. — Coordinate centers are J2000.0, field dimensions are in arcminutes. N_{SRC} gives the number of point sources visible in each field. $N_{non-null}$ is the subset of N_{SRC} that are found within $2''$ (for $w1$ and $w2$) or $3''$ (for $w3$ and $w4$) in the *AllWISE* catalog with non-null photometric error.

Table 2. *WISE* Potential 90% Completeness Limits

	W3		W5	
Band	Low Sky	High Sky	Low Sky	High Sky
1	14.75	12.25	14.75	14.75
2	14.75	11.75	14.25	14.25
3	10.75	8.25	11.25	9.25
4	6.25	3.25	7.25	5.75

$w2$) or 3″ (for $w3$ and $w4$) with non-null photometric error (the $w?sigmpro$ column in the online table). We calculate the 90% magnitude completeness limit of the *AllWISE* source extraction in these test fields by comparing histograms of source magnitude of *AllWISE* objects that match the truth catalog (so as to filter off spurious detections), to the *Spitzer* catalogs for the same regions. The completeness estimates for *AllWISE* are presented in Table 3.

2.3. Fake Source Contamination in *AllWISE*

The 'truth' catalog allows us to estimate the rates of contamination by fake sources in the *AllWISE* point source catalog by band, on and off cloud in areas of high and low sky background respectively. In each test field we search for objects within 2″ (for $w1$ and $w2$) or 3″ (for $w3$ and $w4$) of our by-eye source lists. In Table 4 we present the number of objects that match the truth catalog with signal to noise ≥5 in that band, in high and low sky regions, versus the number of objects with signal to noise ≥5 in *AllWISE* that have no visible point source in that band in the test fields. In low sky regions, the contamination in $w1$ and $w2$ is ≈10%, but in high sky regions about 1/3 of sources above a signal to noise ratio (SNR) of 5 appear spurious. In the $w3$ and $w4$ bands, the vast majority of sources above SNR=5 in the *AllWISE* catalog are likely spurious detections and simply represent upper limit measurements of the nebular background. At the same time, adding up the total number of real sources in Table 4, or looking at the final column in Table 1 also shows that in bands 1 and 2 only about 1/3 of all the sources visible in the images are detected by *AllWISE* at all (compare N_{SRC} and $N_{non-null}$ in Table 1). In band 3, *AllWISE* picks up 50–60% of truth catalog sources, while in band 4, *AllWISE* finds about 3/4 of truth catalog sources. We now look for parameters in the *AllWISE* data release that can help mitigate its unreliability as a YSO finding tool if used incautiously. At the same time we attempt to maintain a high retrieval rate of real sources.

We note that photometric quality flags that designate sources as upper limit detections

Table 3. *AllWISE* 90% Completeness Limits

	W3		W5	
Band	Low Sky	High Sky	Low Sky	High Sky
1	13.75	11.75	13.25	13.25
2	13.75	10.75	13.25	13.25
3	9.25	8.25	10.25	9.25
4	5.25	3.75	7.25	5.75

exist in the *AllWISE* catalog in the *ph_qual* column. But by requiring sources have non-null photometric error as a first, basic requirement, we already implicitly allow *ph_qual* to be only 'A', 'B' or 'C' in that band, or equivalently SNR>2. In the key challenge of suppressing the huge amount of fake detections in bands 3 and 4, even requiring only *ph_qual* 'A' sources only reduces the contamination rate to 85% and 94% respectively. In bands 1 and 2, the contamination rate is already quite low (Table 4) and would only drop by a few percent by requiring *ph_qual* = 'A' only.

3. *AllWISE* Fake Source Mitigation

3.1. *AllWISE* Catalog Parameters and their Properties in Real and Fake Sources

3.1.1. Signal-to-noise and Chi-squared

The signal to noise ($w?snr$) and reduced chi-squared ($w?rchi2$) parameters given in the *AllWISE* photometric catalog give a strong discriminating power between real and fake point sources. The behavior of $w?rchi2$ versus $w?snr$ in the two test fields in the four *WISE* bands is shown in Figure 1 and in the Appendix: Figure 20. Hereafter we use χ^2_ν and SNR to refer to reduced chi-squared and signal to noise respectively.

In general, the behavior seen in Fig. 1 is consistent with the expectation that a true point source will have $\chi^2_\nu \approx 1$ from the profile fitting procedure. Fake sources have $\chi^2_\nu \approx 1$ at low signal to noise, but start to deviate away as the measured signal to noise increases. When examined in the *WISE* images, real sources with $\chi^2_\nu > 2$ are crowded by nearby neighboring sources, are in regions of complex and/or bright background emission, or are extended.

We apply the following cuts in SNR vs. χ^2_ν space as shown in Fig. 1:

Table 4. *AllWISE* Fake Source Contamination

Band	High Sky Bkgd. Contamination				Low Sky Bkgd. Contamination			
	W3		W5		W3		W5	
	N_{real}/N_{fake}	$\%fake$	N_{real}/N_{fake}	$\%fake$	N_{real}/N_{fake}	$\%fake$	N_{real}/N_{fake}	$\%fake$
1	400/209	34.3	143/79	35.6	94/19	16.8	460/62	11.9
2	344/176	33.8	163/84	34.0	122/15	10.9	414/32	7.2
3	208/2457	92.2	158/2081	92.9	168/485	74.3	293/62	75.8
4	135/5526	97.6	169/5554	97.0	168/2435	93.5	133/2379	94.7

$$w1rchi2 < (w1snr - 3)/7 \quad (1)$$
$$w2rchi2 < 0.1 \times w2snr - 0.3 \quad (2)$$
$$w3rchi2 < 0.125 \times w3snr - 1 \quad (3)$$
$$w4rchi2 < 0.2 \times w4snr - 2 \quad (4)$$

to suppress the fake component. These criteria also allow some fraction of the real sources with high χ^2_ν to be included. We tabulate the retrieval rate of real sources and the residual contamination rate by spurious catalog entries in Table 5. In this and the following sub-sections our starting point for the retrieval rate is the final column of Table 1, so we implicitly always require that *AllWISE* sources in a given band have non-null photometric uncertainty *w?sigmpro*. For example, in band 1 in the W3 test field, Table 1 shows that we find 501 real sources with non-null *w?sigmpro*. Table 5 shows that ≈57% of these sources are retrieved by the band 1 SNR vs. χ^2_ν cut, and 3% of all the *AllWISE* sources that have non-null *w?sigmpro* and pass this cut are fake. With these parameters it is possible to suppress the contamination rate in any band down to < 7%, although this success comes at a cost of cutting about 2/3 of the real sources in bands 3 and 4.

3.1.2. w?nm and w?m

The catalog parameters *w?nm* (the number of profile-fit flux measurements for a source with *w?snr* > 3) and *w?m* (the number of profile-fit flux measurements for a source) also have some potential for separating real and fake sources in the catalog. We might expect that a real point source would be detected with *w?snr* > 3 in a higher fraction of the *WISE* frames. Figure 21 in the Appendix shows the behavior of real and fake sources in these parameters. Table 6 presents a summary of the results of requiring *w?nm*/*w?m* > 0.2. In practice, *WISE* band 4 shows the largest percentage of fake sources with low *w4nm*/*w4m* that might be filtered off by such a search criterion.

3.1.3. nb and na

The catalog flags *na* and *nb* indicate whether a source has been actively deblended (*na* = 0 means no, '1' indicates yes) and if so, how many blend components were used (*nb*). Requiring *nb* = 1 automatically produces *na* = 0. Setting *na* = 0 does not produce *nb* = 1 however, since *nb* can be greater than 1 if a source was passively deblended. Table 7

Table 5. Signal to Noise and Chi-squared

Band	Real Retrieval Rate (%) W3	W5	Residual Fake (% of total) W3	W5
1	56.9	74.8	3.1	3.8
2	60.0	78.3	5.5	4.8
3	23.7	32.1	4.3	6.4
4	41.1	34.3	1.4	6.5

Note. — Retrieval rates are given as the percentage of the real 'truth' catalog sources found in *AllWISE* with non-null photometric error, that are retrieved by the $w?rchi2$ versus $w?snr$ selection criteria in § 3.1.1. The residual fake columns are the percentage of all the sources allowed through by these criteria that are still fake/spurious.

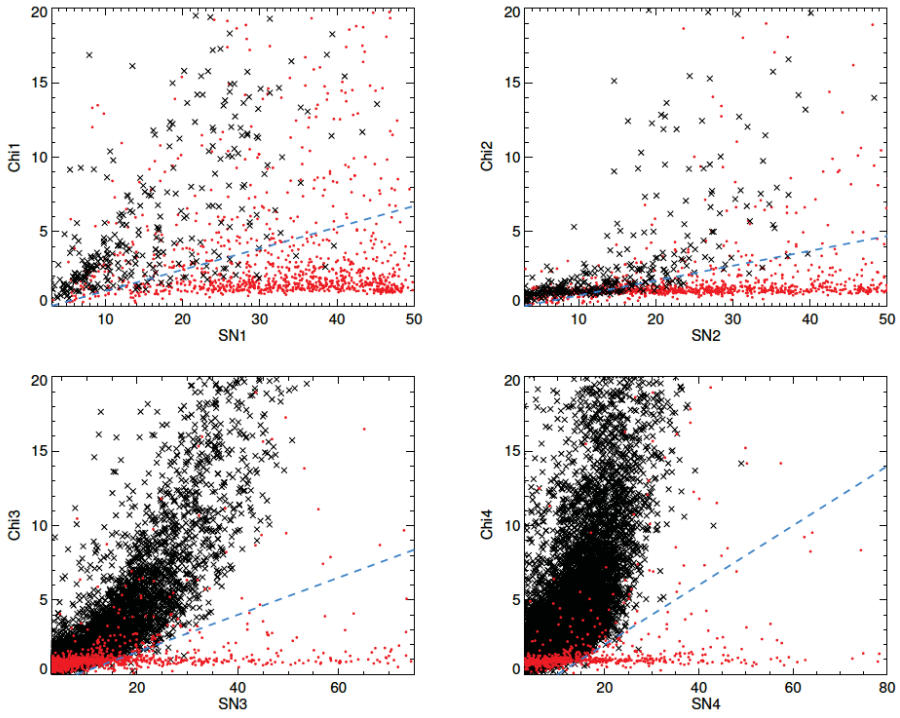

Fig. 1.— The distribution in signal to noise and profile fit reduced chi-squared of truth catalog point sources found in *AllWISE* (red points) and unmatched, spurious *AllWISE* catalog entries (black ×-points) in the four *WISE* bands. Blue dashed line shows the selection cuts we use in this paper.

summarizes the behavior of real and fake sources by band and field. We list the fractions of sources with $nb = 1$ and non-null photometry in each band, noting however, that nb is defined once for each catalog entry and is not separately computed for each band. In general, real sources are more likely to be unblended, but the level of suppression of fake sources in bands 3 and 4 is modest and in bands 1 and 2 comes at the cost of cutting about 30% of real sources.

3.1.4. cc_flags

The confusion and contamination flag (cc_flags) parameter indicates if a source is a likely diffraction spike (D), scattered light halo (H), image latent (P) or optical ghost image artifact (O). Table 8 lists the fraction of sources by band and field that have any of the flags 'D', 'H', 'O' or 'P' in that band. These flags show that only a small and comparable percentage of real and fake sources are flagged as any one of these image contaminants in these fields.

3.1.5. Profile Fit versus Aperture Magnitudes

The *AllWISE* catalog provides magnitudes calculated from the profile fit process ($w?mpro$) and also from curve-of-growth corrected aperture photometry ($w?mag$). Real and fake sources show different distributions in the difference between the profile fit and aperture magnitude values as shown in the Appendix in Figure 22. In Table 9 we present the retrieval rates and residual contamination using a simple trial cut, requiring: $|w?mag - w?mpro| < 0.5$. Figure 22 and Table 9 show that in bands 1 and 2 real and fake sources are more easily separated by a cut based on the difference between aperture and profile fit magnitudes. However in bands 3 and 4 the large spread in $|w?mag - w?mpro|$ of real sources and the large quantity of fake sources with $|w?mag - w?mpro| \sim 0.5$ makes such an approach uneffective.

3.2. An Approach to Mitigating Contamination

In this paper, our goal is to search for young stars with infrared excess emission which, given the techniques laid out in K12, requires that we obtain reliable photometry in at least 3 bands. The key parameters that appear to have the strongest discriminatory effect in suppressing fake source contamination in *WISE* bands $w3$ and $w4$ are SNR and χ^2_ν. While combining many parameters to reduce fake sources as much as possible is appealing, the

Table 6. $w?nm$ and $w?m$

Band	Real Retrieval Rate W3	Real Retrieval Rate W5	Residual Fake (% of total) W3	Residual Fake (% of total) W5
1	99.8	100	32.7	19.1
2	94.5	96.1	28.9	16.5
3	87.5	83.8	89.1	87.6
4	90.1	87.8	96.3	96.4

Note. — Retrieval rates are given as the percentage of real 'truth' catalog sources found in *AllWISE* with non-null photometric error, that are retrieved with $w?nm/w?m > 0.2$ in a given band and test field (see § 3.1.2). The residual fake columns are the percentage of all the sources that are selected by these criteria that are still fake/spurious.

Table 7. nb and na

Band	Real Retrieval Rate W3	Real Retrieval Rate W5	Residual Fake (% of total) W3	Residual Fake (% of total) W5
1	69.7	68.3	20.3	11.2
2	68.9	68.8	18.0	8.4
3	84.5	83.1	84.2	81.7
4	84.1	78.5	96.3	96.3

Note. — Retrieval rates are given as the percentage of real 'truth' catalog sources found in *AllWISE* with non-null photometric error, that have nb=1 (see § 3.1.3) in a given band and test field. The residual fake columns are the percentage of all sources that are selected by these criteria that are still fake/spurious.

Table 8. cc_flags

Band	Real W3 % DHO or P	Real W5 % DHO or P	Fake W3 % DHO or P	Fake W5 % DHO or P
1	2	1	1	1
2	6	1	9	5
3	3	1	4	1
4	8	2	13	5

Note. — Data show the percentage of either 'truth' catalog sources or fake sources in the *AllWISE* catalog that have any of the confusion and contamination flags D, H, O or P in a given field and band.

cost would be to sacrifice real sources we are interested in. Our approach is thus to mitigate contamination using only the criteria based on signal to noise and profile-fit reduced chi-squared. As noted in § 3.1.1, the retrieval rate of real sources in bands 3 and 4 is poor using these criteria, so we recover low signal to noise sources in band 3 by allowing sources with $0.45 < w3rchi2 < 1.15$ and $w3snr > 5$, which means our potential retrieval rate of real sources rises to about 60% in $w3$. Although such a decision also brings in a large quantity of fake detections, in our particular application, the observed *WISE* colors of young stars provide an additional discriminant for these objects. We use a $2''$ search radius to find YSOs in the *AllWISE* catalog from the Taurus compilation of Rebull et al. (2010) and the transition disk objects (TDs) in Andrews et al. (2011) and Cieza et al. (2012). Transition disks are a subclass of young star with inner opacity holes in their disks and reduced levels of near infrared and/or mid-infrared excess emission. The color-color diagram shown in Figure 2 shows the distinct locations occupied by these known YSOs and catalog entries with fake $w3$ photometry in our test fields. Thus in searching for YSOs in *WISE* color-space we can avoid regions with a high probability of reliance on a spurious catalog entry.

The uncertainty/signal-to-noise/chi-squared criteria we use in the following work are as follows. The color-magnitude criteria for YSOs follow in § 4.

WISE band 1: non-null $w1sigmpro$ and $w1rchi2 < (w1snr - 3)/7$.

WISE band 2: non-null $w2sigmpro$.

WISE band 3: $w3snr \geq 5$ and either: $w3rchi2 < (w3snr - 8)/8$ OR $0.45 < w3rchi2 < 1.15$ (the approximate 1σ range of real-source $w3rchi2$ below the initial chi-squared-signal to noise cut).

WISE band 4: non-null $w4sigmpro$ and $w4rchi2 < (2 \times w4snr - 20)/10$.

4. The YSO Finding Scheme

With the previously described requirements on catalog parameters in hand, we lay out the YSO identification and classification scheme. The scheme resembles the one described in K12 but contains updates designed to better account for and eliminate potential photometric and astrophysical contaminants. Figure 3 summarizes the entire scheme in a flow chart for reference. The photometric quality criteria for *WISE* bands 1 and 2 are applied at all steps of the scheme and are shown in a separate, preliminary box before any of the classification steps are taken. The other band requirements are used as needed in the scheme as described in the following text.

Table 9. Profile Fit and Aperture Magnitudes

Band	Real Retrieval Rate W3	Real Retrieval Rate W5	Residual Fake (% of total) W3	Residual Fake (% of total) W5
1	61.5	74.3	3.8	1.5
2	62.5	73.2	9.5	5.1
3	45.7	51.2	65.9	63.6
4	63.7	55.5	76.3	77.9

Note. — Retrieval rates are given as the percentage of real 'truth' catalog sources that are retrieved by the selection criteria in § 3.1.5 in a given band and test field. The residual fake columns are the percentage of all the sources that are selected by these criteria that are still fake/spurious.

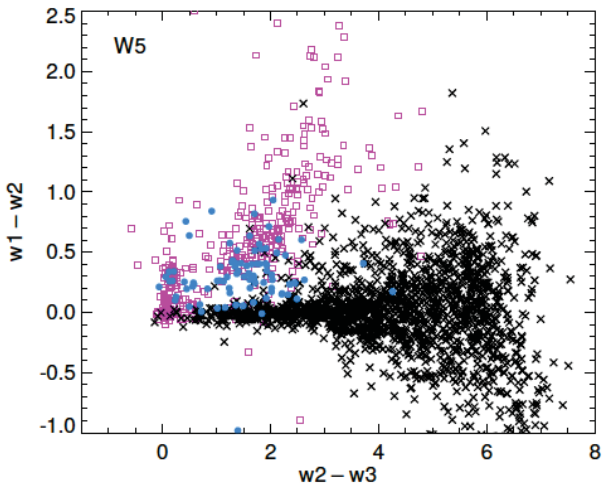

Fig. 2.— *WISE* color-color diagram. Black ×-points are catalog entries with fake $w3$ photometry. Magenta points are Taurus YSOs from Rebull et al. (2010) and blue points are transition disk sources from Andrews et al. (2011) and Cieza et al. (2012) found in the *AllWISE* catalog.

Fig. 3.— Summary flowchart of the YSO identification and classification process in this paper.

4.1. Astrophysical Extragalactic Contaminants

We first remove objects from the catalog that are likely to be unresolved external galaxies. The requirements for their removal are similar to those of K12, but in this case based on sources found in the *AllWISE* catalog around the North and South Galactic Poles, which will likely consist mostly of galaxies and Galactic halo stars. We extract sources from circles of area 100 square degrees centered on the Poles by querying *AllWISE* for sources with $|b| > 84.3558°$. Figure 4 shows a color-color diagram of objects detected in the North polar field (gray points). We overplot tracks showing the location of the galaxy SED templates of Assef et al. (2010). These templates are intended to reproduce the typical components of galaxies: old (E/'elliptical'), intermediate (Sbc/'spiral'), and young stellar populations (Im/'irregular'), as well as nuclear activity (AGN, i.e. active galactic nuclei). Since these selection cuts rely on *WISE* bands 1, 2 and 3, we additionally apply the $w3$ photometry requirement of § 3.2 and remove objects meeting all the following criteria as likely star-forming galaxies ('SFG' in Fig. 3 and the region marked in the left panel of Fig. 4):

$$w2 - w3 > 2.3 \quad (5)$$

$$w1 - w2 < 1.0 \quad (6)$$

$$w1 - w2 < 0.46 \times (w2 - w3) - 0.78 \quad (7)$$

$$w1 > 13.0 \quad (8)$$

Likely broad-line AGN are removed with a color-magnitude cut, see Figure 4 (right panel). We label as candidate AGN those sources that meet the band 1, 2 and 3 requirements and either:

$$w1 > 1.8 \times (w1 - w3) + 4.1 \quad (9)$$

and

$$w1 > 13.0 \quad (10)$$

or

$$w1 > w1 - w3 + 11.0 \quad (11)$$

In these and the following figures, we include arrows representing the extinction vector for $A_{KS} = 0.4$, 0.8 and 2, computed using an interpolation of Figure 1 of McClure (2009). We present our estimated extinction law in the *WISE* bands in Table 10. The vectors shown

in the various figures are not parallel to each other due to the variations in the extinction law as a function of the total extinction as derived by McClure (2009).

4.2. Young Stellar Objects

Having removed the previously defined contaminants, we identify and classify YSOs first using the list of objects that meet the band 1, 2 and 3 requirements. The scheme—as in K12—is developed to follow the observed colors of Taurus region YSOs in Rebull et al. (2010) and transition disk young stars, guided by the catalogs of Andrews et al. (2011) and the compilation of Cieza et al. (2012). To better understand the distribution in *WISE* color-color and color-magnitude spaces of potential astrophysical contaminants to our young star candidates, we use the AGB carbon star catalog of Alksnis et al. (2001), the OH/IR AGB star catalogs of Chengalur et al. (1996), Sjouwerman et al. (1998) and Lindqvist et al. (1992) and the Classical Be stars from Mathew et al. (2008). We search the *AllWISE* catalog within a 2″ search radius for all these object types, requiring their catalog parameters pass our signal to noise and χ^2 cuts and plot them in Figure 5 (young stars in the left panel and other object types in the center panel). To guide the large scale classification of AllWISE data, we also extract a large section of the Outer Galaxy ($105 < l < 153$, $|b| < 5$, hereafter: the Outer Galaxy strip) to examine how these different object types manifest themselves in the catalog (Fig. 5 right panel). In contrast to Fig. 4, several additional clouds of sources can now be seen in the right panel of Fig. 5. The extragalactic objects are still obvious and present, but are now joined by Galactic young stars and the other Galactic object types with infrared excess seen in the left and center panels of the figure. The streak of objects with roughly zero $w1 - w2$ color but a wide range of $w2 - w3$ color are a mix of source types. They may be objects with fake band 3 detections that slip through the photometric quality criteria of § 3.2. They may also be foreground photospheres/main sequence stars with a coincidental background galaxy that gives them an apparent red color. Finally, some fraction may be young transition disk stars, or older, evolved 'debris disk' stars similar to Vega (see for example, Dominik & Decin 2003).

Table 10. $WISE$ Extinction Law

Band	$A_\lambda/A_{KS}(A_{KS} \leq 0.5)$	$A_\lambda/A_{KS}(0.5 < A_{KS} \leq 1)$	$A_\lambda/A_{KS}(A_{KS} > 1)$
1	0.44	0.54	0.67
2	0.26	0.344	0.51
3	0.248	0.37	0.506
4	0.155	0.27	0.43

Class I YSOs (candidate protostars) are the reddest objects, and are classified as such if their colors match:

$$w2 - w3 > 2.0 \quad (12)$$

and

$$w1 - w2 > -0.42 \times (w2 - w3) + 2.2 \quad (13)$$

and

$$w1 - w2 > 0.46 \times (w2 - w3) - 0.9 \quad (14)$$

and

$$w2 - w3 < 4.5 \quad (15)$$

These requirements modify the scheme of K12 to better reflect the divisions in SED slope ($\alpha = d\log(\lambda F_\lambda)/d\log\lambda$, Greene et al. 1994) on which the Class system is based and to eliminate contamination by spurious detections in *WISE* band 3.

Class II YSOs (candidate T Tauri stars and Herbig AeBe stars) are classified from the remaining pool of objects if their colors match the following criteria:

$$w1 - w2 > 0.25 \quad (16)$$

and

$$w1 - w2 < 0.9 \times (w2 - w3) - 0.25 \quad (17)$$

and

$$w1 - w2 > -1.5 \times (w2 - w3) + 2.1 \quad (18)$$

and

$$w1 - w2 > 0.46 \times (w2 - w3) - 0.9 \quad (19)$$

and

$$w2 - w3 < 4.5 \quad (20)$$

As can be seen in Figure 5, the revised Class II criteria attempt to avoid the AGB stars seen in the catalog of Alksnis et al. and the region occupied by Classical Be stars to the blue. This latter region is also where some AGB stars reside, as well as Class III/weak disk YSOs and blue transition disks (Cieza et al. 2012). The criteria also attempt to eliminate a region likely dominated by the reddest star forming galaxies to the lower right in this color-space.

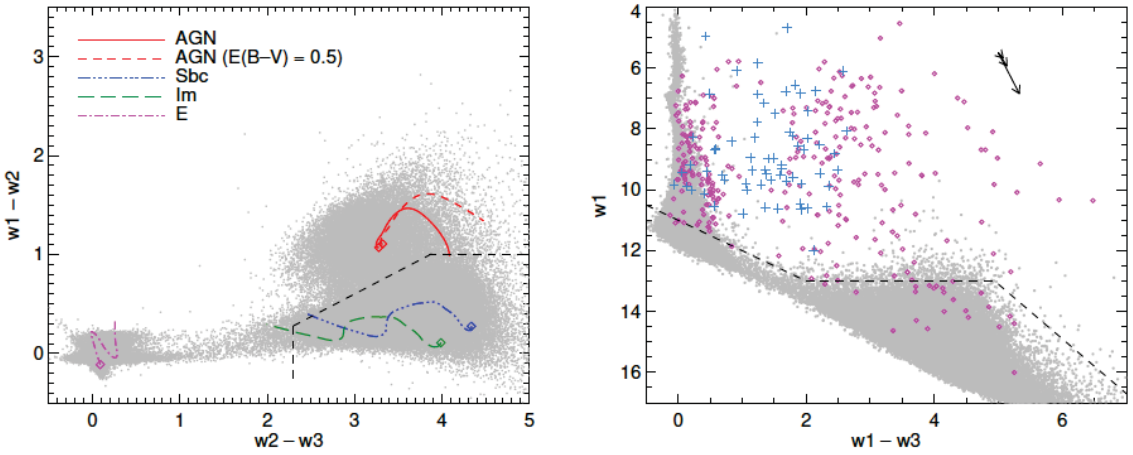

Fig. 4.— Color-color and color-magnitude diagrams of *AllWISE* sources found the North Galactic Pole (gray points). Left panel: we overlay theoretical SED template tracks of galaxy components from Assef et al. (2010). Right Panel: Magenta points are Taurus YSOs from Rebull et al. (2010) and blue points are transition disk sources from Andrews et al. (2011) and Cieza et al. (2012). The dashed black lines mark the regions excluded from our YSO selection. Arrows show extinction vectors of $A_{KS} = 0.4$, 0.8 and 2.

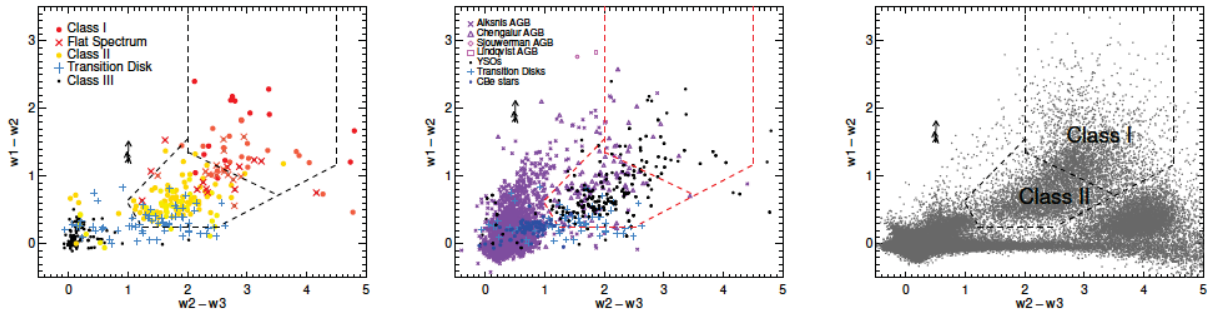

Fig. 5.— *WISE* color-color diagrams. Left panel: Taurus YSOs from Rebull et al. (2010) found in *AllWISE* and blue crosses: transition disks from Cieza et al. (2012). Center panel: AGB stars, CBe stars, YSOs and transition disks, see text. Right panel: Outer Galaxy point sources from *AllWISE* found in region defined by $105 < l < 153, |b| < 5$. All objects shown meet the $w1$, 2 and 3 requirements of § 3.2. Dashed lines show our YSO class divisions. Arrows show extinction vectors of $A_{KS} = 0.4$, 0.8 and 2.

4.2.1. YSOs found with 2MASS and WISE

To compensate for the relative drop in sensitivity in *WISE* bands 3 and 4, both intrinsic and due to the bright background emission at these wavelengths, we use the *2MASS* JHK_S point-source catalog (Skrutskie et al. 2006) that is automatically provided with the *AllWISE* catalog. Here we alter the scheme from K12 and use the $H - K_S$ vs. $w1 - w2$ color-color diagram to find and classify YSOs. In $H - K_S$ vs. $w1 - w2$ color-color space there is less overlap between the reddening vector due to extinction and that due to dust excess emission (see Figure 6). In other words, it is easier to define a line that follows the standard extinction law that excludes most extragalactic contamination for the $H - K_S$, $w1 - w2$ plot than it is in the $K_S - w1$, $w1 - w2$ plot, where reddened background galaxies and main-sequence stars may easily have colors resembling disk excess sources.

One further alteration we make to the scheme of K12 and the original *Spitzer-2MASS* concept of Gutermuth et al. (2009) is to not apply any dereddening to the colors of sources we classify. Lacking an independent method to remove the foreground extinction to each source, or an extinction map, we develop our selection and classification based on the raw photometry. In general, in the Outer Galaxy, line of sight extinction due to dust in between the Solar System and the main star forming regions is low, for example Hillwig et al. (2006) derive an extinction $A_V \approx 2$ to the O stars in the H II region cavity of W5. Within star forming regions however, the most embedded young stars can be hidden behind an $A_V > 15$ (for example, Masiunas et al. 2012, who find peak $A_V = 19.8$ in their extinction map of AFGL 490). Thus in general, the extinction vector in $H - K_S$ versus $w1 - w2$ will have a magnitude < 0.3, but could be as large or larger than 1 in the most embedded cases, meaning some of the objects classified as Class I protostars in this part of the scheme could be reddened Class II stars.

We search for YSO candidates using the following criteria amongst previously unclassified objects with non-null photometric error in *2MASS* H and K_S, and which pass the *WISE* band 1 and 2 requirements of § 3.2 and *fail* those for *WISE* band 3:

$$H - K_S > 0.0 \tag{21}$$

and

$$H - K_S > -1.76 \times (w1 - w2) + 0.9 \tag{22}$$

and

$$H - K_S < (0.55/0.16) \times (w1 - w2) - 0.85 \tag{23}$$

and

$$w1 \leq 13.0 \tag{24}$$

These objects are initially classified with the Class II objects. The subset of them that pass the following criteria are grouped with the candidate Class I/protostar objects:

$$H - K_S > -1.76 \times (w1 - w2) + 2.55 \tag{25}$$

The ratio (0.55/0.16) in the criteria above comes from the calculation of the ratio of color-excesses: $(A_H - A_{KS})/(A_{w1} - A_{w2})$ computed for $A_{KS} > 1$, since this gives the greatest slope in the extinction law, and thus the most cautious cut of galaxies in $H - K_S$, $w1 - w2$ space.

4.2.2. WISE 22 μm Photometry

As in K12, we use $w4$ photometry to identify candidate transition disk objects and to retrieve possible protostars from the AGN candidates. Figure 7 shows the location of the search box for transition disk objects. As can be seen, there is considerable overlap between literature transition disks and Class II sources, likely owing to the sensitive dependence of mid-infrared emission on small changes in the dust distribution and disk inclination. These properties make a scheme like this one an imprecise tool for finding these objects. The streak of objects with roughly zero $w1 - w2$ color and a range of $w3 - w4$ colors is similar to the one seen in Fig. 5 and is likely made up of the same types of sources. As can be seen, literature transition disks are typically not as blue in $w1 - w2$ as this streak, so we avoid this portion of color-color space. We select candidate transition disks with the following criteria, from the sources that meet the requirements on all four bands given in § 3.2.

$$w3 - w4 > 1.5 \tag{26}$$

and

$$0.15 < w1 - w2 < 0.8 \tag{27}$$

and

$$w1 - w2 > 0.46 \times (w2 - w3) - 0.9 \tag{28}$$

and

$$w1 \leq 13.0 \tag{29}$$

The last two criteria attempt to mitigate the contamination by background galaxies

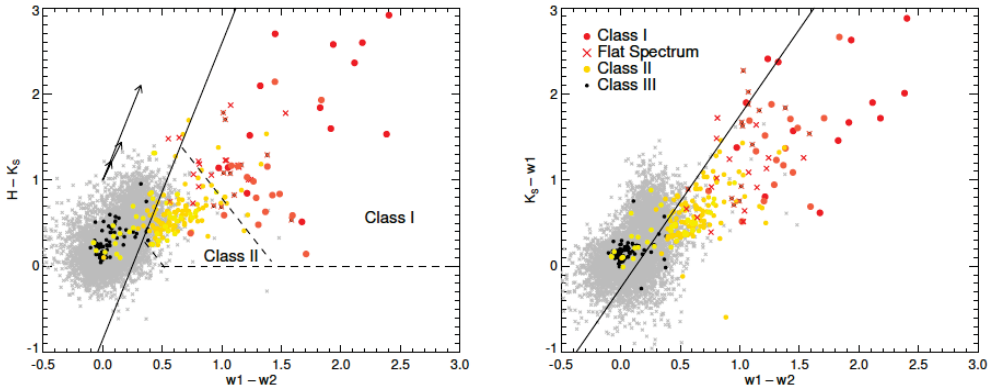

Fig. 6.— *2MASS-WISE* color-color diagrams. Gray points: point sources around the North Galactic Pole. Colored points: YSOs from Taurus (Rebull et al. 2010). Arrows show extinction vectors of $A_{KS} = 0.4$, 0.8 and 2. Solid black line parallels the extinction vector for the highest range of extinctions tabulated in Table 10. Dashed lines in left panel show the YSO Class divisions.

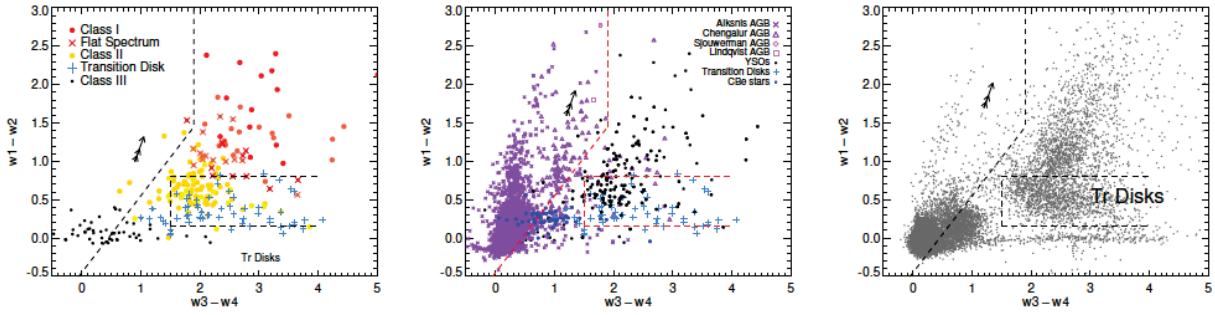

Fig. 7.— *WISE* 4-band color-color diagrams. Left panel: Taurus YSOs from Rebull et al. (2010) found in *AllWISE* and blue crosses: transition disks from Cieza et al. (2012). Center panel: AGB stars, CBe stars, YSOs and transition disks colored as in Figure 5. Right panel: Outer Galaxy point sources from *AllWISE* found in region defined by $105 < l < 153, |b| < 5$. All objects shown meet the requirements on all four *WISE* bands in § 3.2. Dashed lines show the upper left region excluded to remove OH/IR AGB stars and the color-criteria for finding transition disk candidates. Arrows show extinction vectors of $A_{KS} = 0.4$, 0.8 and 2.

in the same way as with Class II objects. The bluest transition disk objects seen in the literature catalogs are too hard to separate from AGB and CBe stars without follow-up spectroscopy (as in Cieza et al. 2012) and we make no attempt to find them in this work.

AGN occupy a similar part of color space to protostars, but we can retrieve an additional set of those objects as candidate protostars if they have a $w4$ magnitude that makes them brighter than the majority of external galaxies. We take the sample of objects previously classified as AGN candidates and identify new protostars with the following color-magnitude cuts, additionally requiring that they meet the band 4 quality criteria given in § 3.2 (see Figure 8):

$$w4 < 5.0 \quad (30)$$

and

$$4.5 < w2 - w4 < 8.0 \quad (31)$$

and

$$w1 - w2 > 1.0 \quad (32)$$

and

$$w3 - w4 > 2.0 \quad (33)$$

4.2.3. AGB stars and CBe stars

Both AGB stars and CBe stars possess a degree of infrared excess, originating in the circumstellar material around these objects. In the case of AGB stars, these objects are in general much brighter than YSOs, unless they are at great distance or strongly extincted, and have a slightly different distribution in color-color space, with the OH/IR category of AGB stars the most similar to YSOs (a similar finding to Robitaille et al. 2008, using *Spitzer* data). CBe stars in general possess a weaker infrared excess than do YSOs, but can be confused with blue transition disk objects. Our initial *WISE* band 1, 2 and 3 classification of YSOs filters some fraction of these object types. After passing through all the preceding steps, we make one final pass to remove these objects. We use a combination of the *WISE* $w1 - w2$, $w3 - w4$ color-color diagram (see Figure 7) and the $w1$ vs. $w1 - w2$ color-magnitude diagram (Figure 9). An initial run of the classification scheme up to this point on the Outer Galaxy strip described in § 4.2 is shown in the left panel of Figure 9. The prominent clustering of objects with bright $w1$ magnitudes is almost certainly dominated by AGB stars as can be seen in the right panel of the figure. Thus, stars previously classified as any type of YSO are

rejected if they meet the following conditions:

Firstly, any of the YSO candidates from the previous sections that are bright in *WISE* band 1 with:

$$w1 < (-10/3) \times (w1 - w2) + 9 \quad (34)$$

or

$$w1 < (6/7) \times (w1 - w2) + 5.5 \quad (35)$$

or any of the YSO candidates from the previous sections that meet the requirements on all four bands given in § 3.2 and have:

$$w3 - w4 < 1.9 \quad (36)$$

and

$$w1 - w2 < w3 - w4 - 0.45 \quad (37)$$

The right panel of Figure 9 also shows that for nearby regions like Taurus, some bright YSOs may be lost to a cut for AGB stars like this one. In cases like this, analysis of the data for the region considered would be necessary to establish a compromise cut appropriate for the data considered.

4.3. Planetary Nebulae

Unresolved planetary nebulae (PNe) are potentially a source of contamination to the YSO sample, and are considered in § 4.6 when we compute the residual contamination likely from Galactic sources. However, we make no attempt to avoid their detection in this scheme. As can be seen in Figure 10, their typical colors in the *WISE* bands when filtered by our signal-to-noise and chi-squared cuts place them mainly outside the regions occupied by young stars and our selection regions. We draw samples of PNe from a $2''$ search in *AllWISE* for objects in the Macquarie/AAO/Strasbourg Hα (MASH) catalog (Parker et al. 2006; Miszalski et al. 2008), Cohen et al. (2011) and Acker et al. (1992).

A recent paper by Nikutta et al. (2014) used a model of a spherical circumstellar dust shell to predict the location of AGB stars and young stars in *WISE* color-color diagrams. This model leads them to conclude that young stars should be found in the streak of objects

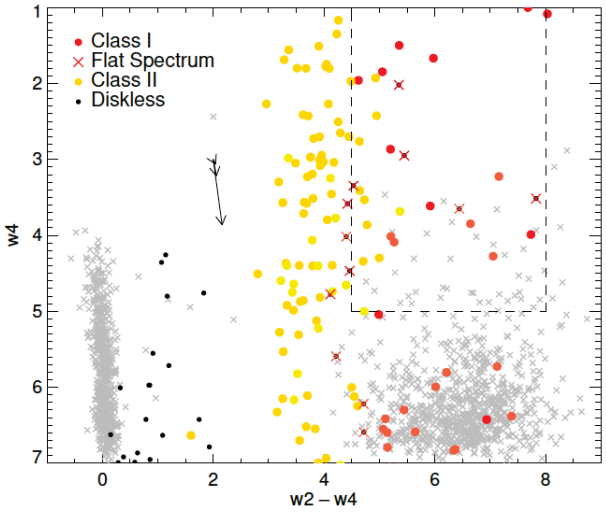

Fig. 8.— *WISE* color-magnitude diagram. Gray points: point sources around the North Galactic Pole. Colored points: YSOs from Taurus (Rebull et al. 2010), colored as before. Arrows show extinction vectors of A_{KS} = 0.4, 0.8 and 2. Dashed box shows region searched for protostars retrieved from AGN sample.

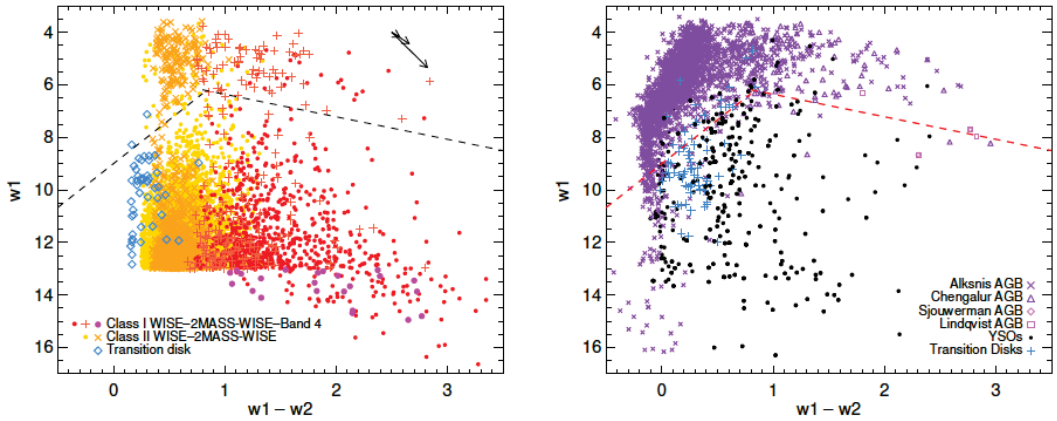

Fig. 9.— *WISE* color-magnitude diagram. Left panel: *WISE* YSO candidates in the Outer Galaxy strip from § 4.2, classified using our scheme. Arrows show extinction vectors of A_{KS} = 0.4, 0.8 and 2. Right panel: literature AGB stars, CBe stars, Taurus YSOs and transition disks. All objects are filtered using our $w1$ and 2 criteria. Dashed lines shows boundary above which we eliminate sources as likely AGB stars.

that we note in sections 4.2 and 4.2.2, which we suspect are more likely to be stars with debris disks (see, for example Morales et al. 2012). Their model also leads them to predict that young stars could be found by searching for objects with $10< w1 <11$, $0.4< w1-w2 <1.4$, and $4< w2-w3 <5.7$. As can be seen in Figure 10, while some Class I young stars will be found by such a search, the majority of this search space is occupied by planetary nebulae.

4.4. Residual Contamination by Fake Photometry

Although the photometric quality requirements in § 3.2 attempt to ensure a reliable source catalog is used to search for young stars, it is possible that at the end of the process of cleaning the *AllWISE* catalog and classifying the sources that some of the YSO candidates are reliant on a spurious detection for their classification.

We test the combined effect of the photometric quality criteria and the YSO identification scheme on our W3 and W5 test fields by classifying the *AllWISE* catalog sources and flagging those where the classification was reliant on a fake detection. We find 1/11 *WISE* Class I's (9%), and 1/76 *WISE* Class II's (1.3%) had a spurious $w3$ detection. None of the YSO candidates relied on a spurious band 1 or 2 detection.

4.5. Application of the Scheme to the Outer Galaxy Strip

Having developed the classification scheme, we test it on the Outer Galaxy strip described in § 4.2. We query the *AllWISE* online database, applying the criteria for $w1$ and $w2$ in the built-in SQL tool, since these apply to all parts of the YSO classification scheme. From an initial 9.1 million catalog sources, we retrieve the following distribution of YSO types shown in Figure 11 and listed in Table 11.

Several notable star forming regions are picked out by the distributions of young stars, in particular (from left to right): AFGL 490, the W5-W4-W3 complex, Cep OB3 (Allen et al. 2012) and the NGC 7538 complex (Ungerechts et al. 2000). The less evolved Class I

Table 11. Galactic Strip YSOs

Class I		Class II		Transition Disk	Embedded Protostars
WISE	*2MASSWISE*	*WISE*	*2MASSWISE*		
750	148	3410	773	45	23

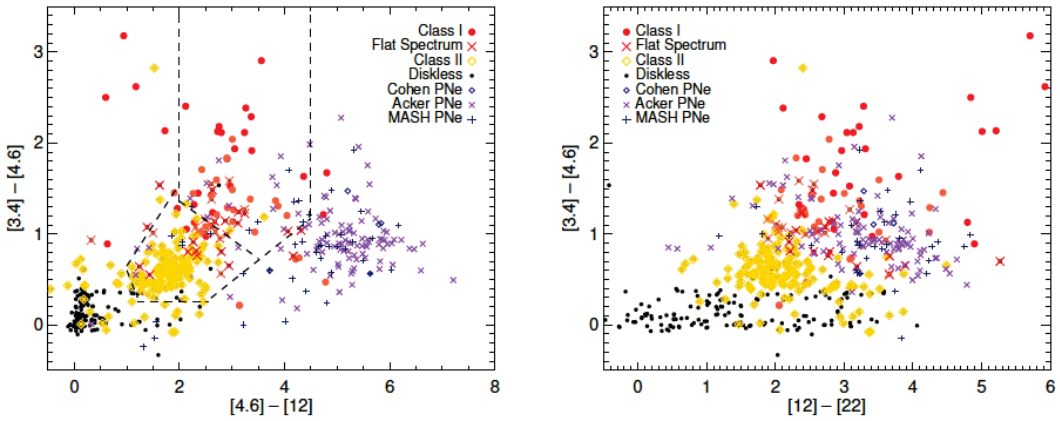

Fig. 10.— *WISE* color-color diagrams showing YSOs from Taurus (Rebull et al. 2010) and PNe from Parker et al. (2006), Cohen et al. (2011) and Acker et al. (1992).

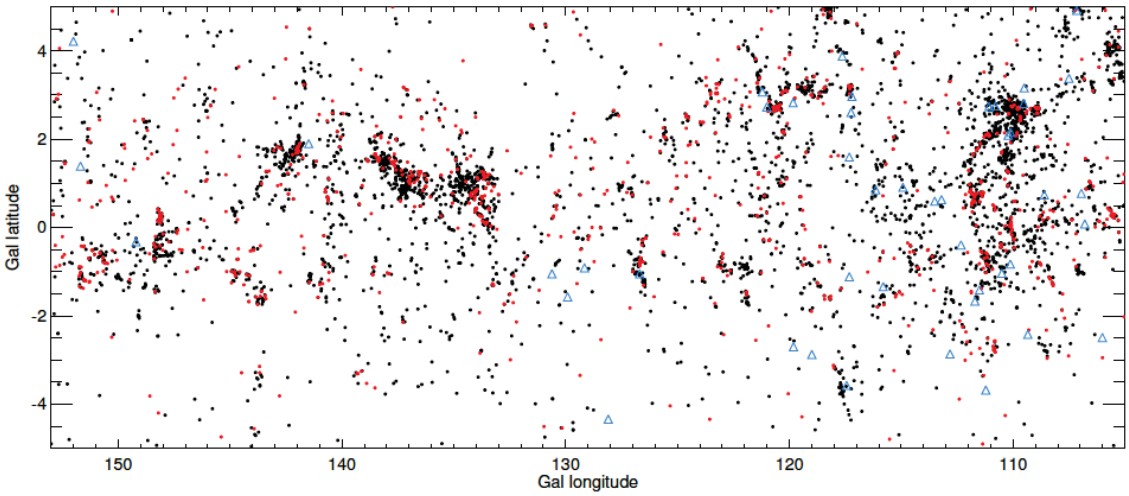

Fig. 11.— Distribution of *AllWISE* detected and classified YSO candidates in the Outer Galaxy. Red points: Class I sources, black points: Class II sources, blue triangles: transition disk candidates.

sources are fewer in number and appear to be spatially concentrated in smaller structures than their neighboring Class II counterparts. We return to this point in a later section.

4.6. Residual Contamination by Galaxies and Galactic Objects

We note that despite the scheme, contaminant astrophysical objects may contribute to the observed distribution of young stars in the Outer Galaxy Strip seen in Fig. 11. To estimate the number of these contaminants we run the following tests.

For external galaxies we download an equivalent area of sky around the North and South Galactic poles (simply searching the *AllWISE* catalog with $|b| > 81.25668$). We randomly place these objects in the Outer Galaxy strip and retrieve the extinction value of the nearest pixel of the Schlegel et al. (1998) extinction map for each object. We redden their *2MASS* and *WISE* photometry according to the extinction law in Table 10 and run the full catalog cleaning and classification scheme. We present the average number of objects that fall into our various YSO class bins in this particular field after 20000 repeats of this process in Table 12. As expected, *WISE*-selected Class I YSOs are the most highly contaminated by galaxies at a rate of about 13%. All other classes are contaminated by external galaxies at a rate of 2% or less.

For Galactic contaminants we use the Galactic populations model of Wainscoat et al. (1992) and the extension to all infrared wavelengths of Cohen (1993) over this field of view, but with no extinction, so the results are an upper limit (a code implementation of this model was kindly supplied by Miranda Dunham and Paul Harvey). We select the following categories of objects from Table 2 of Wainscoat et al. as likely contaminants for confusion with our YSOs in Class I or II by their location in *WISE* or *2MASS-WISE* color-color spaces:

Our Class I objects may be confused with Wainscoat types: X 1E, 2, 3, 4, (the ultra-

Table 12. Probable Extragalactic Contamination in the Outer Galaxy Strip

Class I		Class II		Transition Disk	Embedded Protostars
WISE	*2MASSWISE*	*WISE*	*2MASSWISE*		
96.07	1.81	66.78	8.67	0.002	$< 5 \times 10^{-5}$

Note. — Figures in this table are averages of 20,000 simulation runs computing the number of contaminant extragalactic objects misclassified into the YSO classes presented in this paper. See § 4.6 for details.

luminous 12 μm sources) AGB_CI_01–05, (carbon rich, 'optically invisible' AGB stars with IRAS [12] − [25] color in the range 0.1–0.5) AGB_M_17–25, (oxygen rich AGB stars with IRAS [12] − [25] color in the range 1.7–2.5) PNE BLUE, RED ('blue' and 'red' planetary nebulae).

Our Class II objects may be confused with Wainscoat types: X 1E, (the ultraluminous 12 μm sources with silicate emission) AGB_CI_01–31, (C-rich, 'optically invisible' AGB stars, $0.1 < [12]-[25] < 3.1$) AGB_M_07–15, (O-rich AGB stars, $0.7 < [12]-[25] < 1.5$) RNE BLUE, RED ('blue' and 'red' reflection nebulae).

Since the Wainscoat-Cohen model code allows the user to select which of the different object categories are present in a particular portion of the Galaxy, we use it to generate L-band magnitude histograms for these specific Class I and II contaminants separately, applying our average *WISE* band 1 completeness curve for the W5 test field at the faint end and cutting everything brighter than L=7 (to replicate our AGB exclusion method). This method assumes that the L-band is a good match for $w1$.

Objects in the X1E, AGB_M_07 and 09, AGB_CI_01–11 categories all have colors which mean they would be rejected by our *WISE* $w1 - w2$ vs. $w3 - w4$ category if detected in *WISE* band 4. We remove these from our Galactic contaminant estimation if their apparent IRAS 25 μm magnitude is less than 6 in the final computation (an approximate band 4 completeness cut).

We run the Wainscoat-Cohen model code once for the Class I-like sources and once for the Class II-like sources. We apply an additional faint cut of 13th magnitude for the Class II sources, since these are rejected by the YSO scheme, and derive a final numerical estimate of the total number of non-YSOs that may be in the field of view. We predict 68 Class I and 222 Class II sources at most may be contaminant Galactic objects. Since we do not separate this simulated population of Galactic contaminant objects into the different bins of our classification scheme, these estimates represent $\sim$7.5% and $\sim$5% of the total Class I and Class II YSO candidates found in the Outer Galaxy strip. The robust population of young stars detected by the *AllWISE* catalog and our classification scheme is thus about 730 Class I and 3900 Class II objects.

5. Analysis

5.1. Stellar Clustering

The question of the existence of two distinct modes of star formation, one 'clustered' where stars are formed in groups, associations or true clusters as observed in general in star forming regions, and one 'isolated' has been raised in the literature for decades. For example, Roberts (1957) attempted to calculate whether all O and B stars form in clusters and associations, or whether "individual stars form in the general field." A bimodality in star formation clustering has been suggested to explain, for example, the widespread detection of X-ray bright and presumably, young stars in and around molecular clouds (Carpenter 2000). If an isolated population does exist, a natural question would be to ask if it has different properties to the clustered mode. In this paper, we use the term 'isolated' or 'non-clustered' to specifically refer to a distinct population that is separate from the continuum of cluster sizes that are observed in star forming regions and molecular clouds. If a clustered environment is necessary for the formation of massive stars (see Zinnecker & Yorke 2007 for a discussion of this hypothesis), then the mass function of the isolated population may differ from that of the clustered population, although the calculations of de Wit et al. (2005) show that isolated O stars can be explained by the combined effects of a universal cluster size/density distribution and stellar mass function.

One of the simplest ways to analyze the clustering properties of stars projected onto the sky is to compute the distribution of local surface densities. We compute a proxy for the surface density, μ at the position of each star using the angular distance to the 6th nearest neighbor of each object, s_6. Following Casertano & Hut (1985), the jth surface density estimator μ_j is:

$$\mu_j = \frac{j-1}{\pi s_j^2} \tag{38}$$

where s_j is the distance to the jth nearest neighbor of an object. Casertano & Hut (1985) conclude that choosing $j = 6$ provides the best balance between an accurate computation of density (which would require large j) and a 'local' density estimate, which would call for small j. Thus:

$$s_6 \propto \mu_6^{-2} \tag{39}$$

Since we do not know exactly which of our YSO candidates are background galaxies, or Galactic contaminant objects, we compute an average angular distance distribution, applying

a Monte Carlo style method to subtract off these sources of contamination by repeatedly, randomly removing samples of objects with the same $w1$ magnitude distributions and total number as that predicted previously and re-computing the angular distance distribution. In each iteration we derive a new calculation of the expected contamination due to galaxies. The final averaged angular distance distributions for the Class I sources and for a combined sample of the Class I and II sources are shown in Figure 12 in the left and right panels respectively. Both distributions in Figure 12 peak at small angular distances because of the large fractions of these objects in clusters and aggregates of various sizes. Since our YSO survey is incomplete, the true peaks of the distributions are likely at smaller angular distances than those shown in the figure. The distributions both have tails that extend to large angular distances $>2^{\circ}$, some of which could be explained by a population of very isolated/non-clustered young stars.

We investigate the possibility of a non-clustered population by assuming that such sources would exist in a distribution with some scale height in the Galactic disk. For a simple test, we construct a comparison sample with an exponential distribution in the vertical (latitude) direction and uniform in the plane of the Galaxy. We assign each object an absolute $w1$ magnitude by drawing from the distribution of the c2d catalog sources of Evans et al. (2009), where we match their list to the *AllWISE* catalog and separate their sources into the YSO Class divisions set in § 4. We apply the average W5 $w1$ completeness curve to the resultant apparent magnitude distribution of sources and additionally require objects have $w1 \leq 13$, since our extragalactic filtration technique essentially imposes this cut on our data. In Figure 12, we show the angular distance distributions of these samples where we find an approximate match to the shape of the low density end of the true YSO distribution, separately matching Class I objects (left panel) and a combined Class I and II sample (right panel). Increasing the total number thrown into the sample (with constant scale height) pushes the number of sources at the peak of the curve above the data. Decreasing the total input number produces an excess of sources at very low density/large angular distance (more than a factor of 2). The *WISE* YSO histograms contain on average 760 Class I and 3910 Class II stars after contaminant subtraction. The best matching histograms contain on average 320 sources (left panel) and 1800 sources (right panel). If a uniform, scale height component makes up part of this observed distribution of YSOs in this way, this analysis shows that it is not more than $\approx$1/3 of the total number of sources.

We note that *WISE*'s incompleteness means the observed stellar densities are underestimates (or in apparent nearest neighbor angular distances, overestimates) of the true values. In the prominent star forming regions in Figure 11 are the well-studied regions: AFGL 490 ($(l, b) = (142.0, +1.82)$, distance = 900 pc, Masiunas et al. 2012), Cep OB3 ($(l, b) = (111.26, +2.98)$, d = 700 pc, Allen et al. 2012), W5 ((l, b) = 138, +1.5, d = 2 kpc, Koenig et al.

2008). A 3″ match of our YSO catalog to these published lists of Class I and II sources (excluding transition disks and Class III/weak-line T Tauri stars) retrieves 26% (AFGL 490), 25% (Cep OB3) and 16% (W5) of the *Spitzer*-classified stars. Thus the true stellar densities in these clusters are at least a factor ≈5 greater.

To test if a scale height distributed component could still explain the low density end of the young star density distribution, we crudely imitate the effect of *WISE*'s incompleteness by scaling all the nearest neighbor distances by $1/\sqrt{5}$ and increasing the total number of objects in the histogram by 5. This experiment assumes that we have missed a fixed fraction of the total number of young stars in the Outer Galaxy, whether in or out of massive regions. We repeat the experiment of trying to match scale height distributions of stars to the new, scaled histogram. In this test we apply the *Spitzer* completeness calculation from Koenig et al. (2008) to the sample of sources and apply a faint cut off of IRAC band $1 < 14$ to represent their more lenient galaxy removal technique. Figure 13 shows the results of this trial applied to the combined Class I and II sample. In this case, a smaller fraction—roughly 2400 objects out of the increased YSO count of 23350 stars—can be fit with the uniform component, which also suffers from the problem of over-predicting the number of low density sources (nearest neighbor distance $> 50'$) by a factor of 5. Since *Spitzer* itself is also incomplete to the low mass end of the IMF in this field, and we have only considered those young stars which still possess a visible infrared excess, the fraction of stars in a random, non-clustered population may be lower still.

5.2. Two-point Correlation Function

We compute the two point correlation function (TPCF) of a single output of the contaminant-subtracted sample of YSOs, separated into Class I and II samples. We use the following estimator of the TPCF following Peebles & Hauser (1974):

$$\xi(\theta) = \frac{N_R}{N}\frac{DD(\theta)}{RR(\theta)} - 1 \tag{40}$$

Where DD and RR are the numbers of pairs as a function of angular separation θ in the YSO catalog and in a randomly distributed catalog with 3× the number of objects respectively. We generate $RR(\theta)$ by randomly populating the latitude-longitude range of our test region. In this formulation, a random distribution of sources would have $\xi(\theta) = -2/3$, or $\log(1 + \xi(\theta)) = -0.477$. Figure 14 shows a plot of $(1 + \xi(\theta))$ vs. θ for the Class I and II samples (with logarithmically scaled axes), overlaid with weighted least-squares fits to the roughly linear part of the data (left hand panel). The right hand panel shows the same data

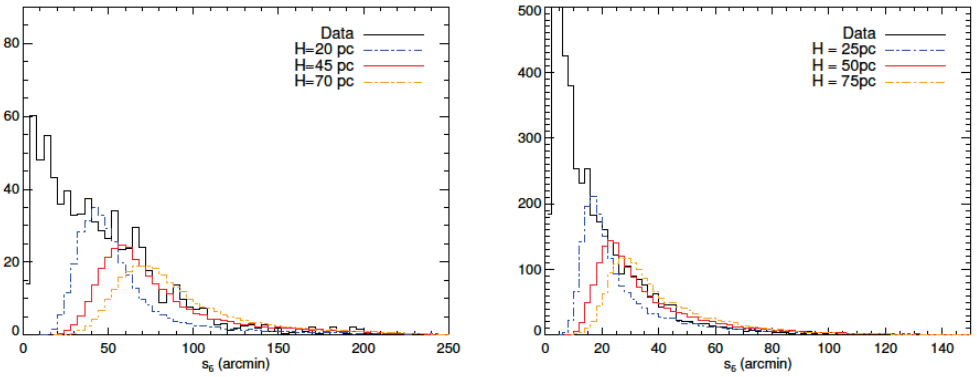

Fig. 12.— Black histogram: 6th nearest neighbor distance s_6 distribution for Class I candidates and combined Class I+II sample after subtracting off computed average distribution of galaxies and Galactic contaminants from Wainscoat et al. (1992). Colored histograms show the scale height distributed samples' s_6 distributions for a range of trial scale heights.

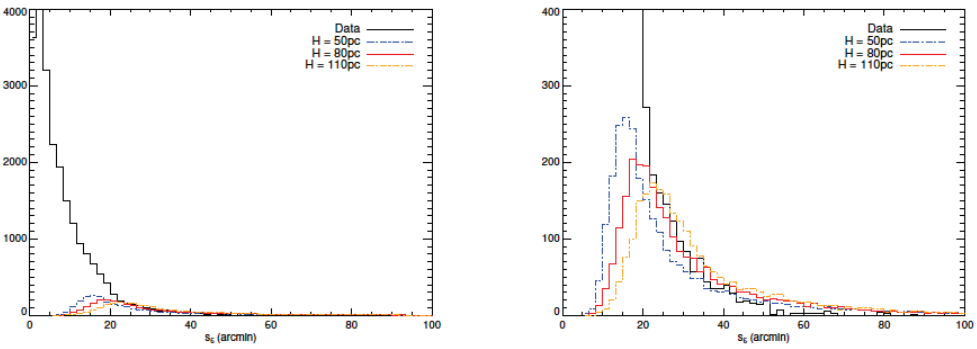

Fig. 13.— Black histograms: 6th nearest neighbor distance s_6 distribution for combined Class I+II samples scaling all distances by $1/\sqrt{5}$ and increasing the total number by 5. Colored histograms show the scale height distribution sample s_6 distributions for a range of trial scale heights. Right panel is a zoom in on the left panel to highlight the differences in the model histograms.

without error bars and unweighted fits to the data between 200 and 4000″.

Both the Class I and II data fall below the random level at separations $\theta \gtrsim 18000''$, or about 5°, likely due to edge effects becoming significant in the calculation of $\xi(\theta)$. The features evident in the data at the longest separations (roughly 100,000″ or 28°) are the result of the real clusters visible in Figure 11. The Class I distribution appears to follow a power law up to separations of about 4000″ or just about one degree. The Class II distribution is shallower, and appears to have a power law shape up to separations $\theta \approx 7000''$ with a turnover at about 200″. As discussed by Kraus & Hillenbrand (2008), work by Larson (1995), Simon (1997) and others has shown evidence that young stars are distributed in a fractal manner with self-similar structure over a range of angular scales in star forming regions like Taurus. Following the methodology of Kraus & Hillenbrand, in a fractal distribution the number of neighbors within angular distance θ goes as $\mathrm{N}(\theta) \propto \theta^D$, where D is the fractal dimension, or the degree to which the distribution fills space. In such a distribution the mean surface density of companions $\Sigma(\theta) \propto 1 + \xi(\theta) \propto \theta^{D-2}$. For the Class I sources the weighted least squares fit technique finds a slope of -0.69 ± 0.06 and thus $D = 1.31$ and for the Class II's a slope of -0.70 ± 0.02 and $D = 1.30$. These slopes are statistically equal, but the fits are strongly skewed to match the data around 2000″ where the error bars are smallest, due to the random distribution peaking around this value of object separations. The unweighted fits (slopes of -0.87 ± 0.02 for the Class I's and -0.72 ± 0.01 for the Class II's) capture the fact the Class I source correlation function falls below the Class II function at scales > 300″, consistent with the more evolved Class II sources being more spread out in space and the younger Class I sources more filamentary and concentrated. This interpretation is consistent with the findings of André et al. (2010) and others who show that star-forming gas as seen in the far-infrared with the *Herschel* space telescope appears to be dominated by filamentary structure. The difference in the intercepts of the straight-line fits in the left-hand panel of Figure 14 is ≈0.17, or a size ratio of about 1.5.

5.3. Cluster Dispersal

One possible contributor to the population of sources outside the prominent, obvious clusters in Figure 11 is the dispersal of young stars from parent clusters or small groupings. The infrared excess emission that allows us to identify candidate young stars has a half life of around 2 Myr, although objects with an infrared disk signature can still be seen in star forming regions as old as 10 Myr (Sicilia-Aguilar et al. 2006). In 5 Myr, a Class II object traveling at a typical velocity of 3 km s^{-1} (Fűrész et al. 2006) would travel about 15 pc. At a distance of 200 pc it would have moved about 4° on the sky, at 1 kpc about 1° and about

$30'$ at a distance of 2 kpc. The combined lifetime for the Class I and Flat SED phase of young stellar objects (Evans et al. 2009) is roughly 1 Myr. At a typical velocity of 1 km s^{-1} (Offner et al. 2009), at a distance of 200 pc it would have moved about $17'$ on the sky, or $\approx 100''$ if at a distance of 2 kpc. Thus it is possible that some of the most isolated young stars in the Outer Galaxy strip are runaways from clusters, in particular the Class II sources. The isolated Class I sources are harder to explain away completely in this manner and some may be genuinely forming in very sparsely populated environments. A more sophisticated model of the distribution of young stars in the Outer Galaxy strip that incorporates cluster dispersal would help us understand exactly how many stars may be forming in isolation. Follow-up observations of the isolated Class I candidates with higher spatial resolution and sensitivity and at other wavelengths would also help understand how many of these objects are cluster escapees or contaminant objects we have not previously accounted for.

6. Discussion

6.1. Filtering the *AllWISE* Catalog in the Galactic Plane

The *AllWISE* photometric filtration scheme presented in this paper is imperfect and ideally researchers would visually inspect *AllWISE* images of objects of interest found in the catalog in all four bands. In the current era where big data is a powerful tool to test theories in new and creative ways, this step may become prohibitively time-consuming, thus the scheme presented here at least allows a first pass to reduce the number of objects that need to be manually checked. It is very important to note that different areas of the Galactic Plane may behave differently than the star-forming test regions analyzed here, particularly the Galactic Center region, where confusion is likely to strongly affect performance. However, the behavior of the various catalog parameters like signal to noise and chi-squared in response to real and spurious sources and objects that are confused or extended is generally applicable. It is certainly important to note the relative strength and weakness of different catalog parameters and we hope to have provided starting points for researchers needing to find a pathway through the *AllWISE* catalog to conduct the source searches and studies they care to do.

6.2. Stellar Clustering

Observations of the distributions of young stars in very large fields with a survey like *WISE* enable us to take steps beyond previous studies of star formation by allowing us

to begin to connect the observations made in nearby galaxies with those of individual star forming regions in our own Milky Way. If a future, complete theory of star formation is to be able to predict the star formation rate and spatial distribution of stars in a large subsection of a galaxy given the gas distribution and kinematics, then we need to have observations of the large scale distribution of star formation in similar sized regions against which to test such a theory. Our observations in this paper, while limited by the properties of the *WISE* survey, provide a beginning to the process of extracting and analyzing a full census of star formation in a large portion of a spiral galaxy.

Our first observation of the distribution of the stars in our sample extracted field shows an obvious degree of clustering into large regions, but with a lower density population between them. We have found that when considering this large scale distribution of young stars in the Outer Galaxy, at most about 1/3 of stars can be fit with a simple scale height distribution. We argue that this means that it is a true statement that the majority of stars form in a clustered environment, that is to say, in prominent massive star forming regions whose density distribution is sharply peaked towards high densities. However, we have also shown that, in a simple test to correct for *WISE*'s incompleteness with respect to hypothetical *Spitzer* Space Telescope observations, the size of the isolated or non-clustered or scale height component may be a much smaller fraction of the total distribution of stars, and may not be required at all. The fact that the low density end of the distribution of stars observed with *WISE* appears to be well fit with a scale height similar to that of OB stars ($\sim$50 pc, Reed 2000) and molecular gas ($\sim$70 pc, Cox 2005) in the Galactic Plane may simply reflect the fact that *WISE* only detects a small fraction of the true population of young stars. Since the *WISE* survey in this paper is magnitude-limited, we tend to include distant, bright objects and miss their possible neighboring cluster members. The $\approx 6''$ resolution of *WISE* also becomes significant for more distant young stars. At 2 kpc $6''$ equates to a distance of 0.06 pc. At 3 kpc this resolution is 0.09 pc, which is approaching the median separation of stars in Taurus (about 0.17 pc, from a simple computation of nearest neighbor distances for the sample of Hartmann et al. 2005). Thus the observed clustering properties of more distant stars may reflect only the smooth, large scale distribution of the gas and may miss their true nature as part of the continuum of cluster sizes.

The largely hierarchical nature of the distribution of stars is also reflected in the power law shape of the two-point correlation function, $\xi(\theta)$. The break in the power law at roughly 2° may also indicate a transition to isolated star formation. As can be seen in our data, two degrees is approximately the size of regions like W5, W3 and 4 and Cep OB3.

As described in § 5.3 it is possible that some fraction of the apparently isolated young stars we see are the dispersed members of young groups or clusters, in particular the Class

II sources and especially if there are a large quantity of objects within 500 pc. The isolated protostars are harder to explain in this way as dispersed cluster members, however since they are younger they are more likely to be concentrated in physically small regions, like the star-forming pillars around H II regions (e.g. Koenig et al. 2008). As we probe deeper, with higher resolution observations and gain more information about stellar proper motions, it may be that further observations of the low density population reveal all young stars to be part of a single cluster continuum. We intend to pursue this approach with a forthcoming study combining data from the *Spitzer GLIMPSE360* Galactic Plane survey with *WISE* to examine the distribution of these stars when observed at higher spatial resolution and sensitivity.

The work of Bressert et al. (2010) and others has already shown that within star forming regions, there is no obvious break in the density distribution of young stars that would indicate a separate, isolated component. If higher resolution and sensitivity observations do indeed bear out the result that a truly distinct, isolated population is either small or non-existent, this would be consistent with the work of Hopkins (2013) who argues that observed density distributions of young stars are simply a continuum resulting from the imprint of the hierarchical nature of supersonic turbulence in molecular clouds (although as noted by Krumholz 2014, Klessen & Burkert 2000 also produce hierarchical structure in star forming gas without turbulence) over all scales. In this picture, isolated (or at least, apparently isolated) star formation would represent $< 10\%$ of the total in a single, unified mechanism of star formation. If a truly isolated population is supported by future observations, however, it will be interesting to scrutinize its origins and mass function.

7. Conclusions

We have presented an assessment of the performance of *WISE* and the *AllWISE* data release in a search for YSOs in a section of the Galactic Plane. We have derived general results for the completeness of the survey and this particular point source extraction in the presence of modest clustering and bright nebular backgrounds. We have also demonstrated the properties of real and spurious detections in the *AllWISE* catalog and their behavior in several key parameters provided in the catalog. We hope these will provide guidance to researchers intending to use the point source catalog in Galactic Plane regions.

We present one approach to improve the source reliability in the four *WISE* bands with signal-to-noise and chi-squared cuts and we use the resulting catalog to construct a new, revised young star detection and classification scheme combining *WISE* and *2MASS* near and mid-infrared colors and magnitudes.

We apply this scheme to a section of the Outer Milky Way and assess the clustering properties of the resulting distribution of Class I and II stars using a 6th nearest neighbor density calculation and the construction of the two-point correlation function. Our analysis suggests that indeed, the majority of stars do form in massive star forming regions, and any isolated mode of star formation is at most a small fraction of the total star forming output of the Galaxy. We also show that the isolated component may be very small and might thus represent the tail end of a single mechanism of star formation in line with models of molecular cloud collapse with supersonic turbulence and not a separate mode all to itself.

In the near future, we will test these results with the addition of higher resolution and sensitivity data from *GLIMPSE360* to examine how the low density population is distributed and clustered. We will also use available *Herschel* data to look at the properties of the interstellar medium near these objects.

Further in the future still, measurements of the distances and kinematics of these stars with the recently launched *Gaia* space mission will allow us to overcome some of the limits of our magnitude limited approach and give a more complete census of the diskless population that may accompany the Class I and II sources we detect here. Proper motion measurements made by *Gaia* of a significant fraction of the young stellar objects seen in our survey will enable a test of the fraction of the isolated population contributed by dispersed and ejected cluster or group members.

We thank an anonymous referee, whose comments and suggestions improved the paper. Author Koenig gratefully acknowledges support from NASA ADAP grant number NNX13AF07G. This work is based on data obtained from (1) the *Wide-Field Infrared Survey Explorer*, which is a joint project of the University of California, Los Angeles, and the Jet Propulsion Laboratory (JPL), California Institute of Technology (Caltech), funded by the National Aeronautics and Space Administration (NASA); (2) the Two Micron All Sky Survey,a joint project of the University of Massachusetts and the Infrared Processing and Analysis Center (IPAC)/Caltech, funded by NASA and the National Science Foundation; and (3) the NASA/IPAC Infrared Science Archive, which is operated by JPL, Caltech, under a contract with NASA. This research has made use of NASA's Astrophysics Data System.

A. Appendix

A.1. Completeness

We derive the completeness, by band, on and off cloud (i.e. in regions of high and low sky background) in two test regions covering W5 and W3/W4. We define high and low sky regions by a threshold sky value (as given in the *AllWISE* catalog) that as best as possible traces the observed cloud boundaries in our *WISE* mosaic images when catalog sources are over plotted and color-coded according to their listed local sky value. These thresholds in sky background value in digital numbers are listed in Table 13. Figure 15 shows plots of *AllWISE* catalog sources in the test fields color-coded in this way, showing high (red) or low (blue) sky emission regions.

A.1.1. WISE Potential Completeness

To derive a value for the completeness in each band, we extract *Spitzer* photometry from Koenig et al. (2008) in W5 and an extraction of photometry from data in the *Spitzer* Heritage Archive for W3/W4 in IRAC bands 1, 2 and 4 and MIPS 24 μm corresponding roughly to the four *WISE* bands respectively. Each source in the *Spitzer* lists is assigned the sky value of the nearest object in the *AllWISE* catalog. We match our manually generated *WISE* source list to the *Spitzer* catalogs with a $2''$ search radius to determine what fraction of the *Spitzer* objects could be detected by *WISE*. Figure 16 shows the histograms of the *Spitzer* catalog and potential-*WISE*-retrieved subset, separated by field, by high or low sky background and by band. We then plot the 'detected' fraction (and Poissonian error on the fraction) as a function of *Spitzer* magnitude by field and band in Figure 17. The magnitude where the error bar crosses the 90% completeness line is our completeness limit.

Table 13. Sky Threshold Values

Band	W3	W5
1	45	42
2	55	50
3	2050	2040
4	555	562

A.1.2. AllWISE Completeness

The *AllWISE* source extraction pipeline is only able to retrieve a subset of the sources visible in Galactic Plane *WISE* images. We calculate the completeness of the *AllWISE* source extraction by comparing histograms of source magnitude of *AllWISE* objects that match the truth catalog (so as to filter off spurious detections), to the *Spitzer* catalogs for the same regions. Figure 18 shows the histograms of the *Spitzer* catalog and the *AllWISE* 'real' sources over the same area of the test regions. The mismatch in the histograms (for example the W5 $w1$ high sky background plot in upper right) is largely due to the binning in the plots and slight differences in the magnitudes between *WISE* and *Spitzer*, but may also be due to differences in how the background subtraction is handled or source variability. In the $w3$ plots on the third row, *WISE* is able to detect bright objects that are saturated in *Spitzer* images, the bandpasses are less similar and spectral features (e.g. the 10 μm silicate feature, which can vary with evolutionary stage, Kessler-Silacci et al. 2005) in these young objects' infrared spectra may cause other mismatches. We plot the *AllWISE*-detected fraction (and Poissonian error on the fraction) as a function of *Spitzer* magnitude by field and band in Figure 19. The magnitude where the error bar crosses the 90% completeness line is our completeness limit.

A.2. Properties of Real and Fake Sources in the *AllWISE* Catalog

Here we show the plots of the various catalog parameters analyzed in this paper and discussed in § 3 and their behavior in the 'real' by-eye source list and 'fake' sources found in the *AllWISE* Catalog. Black and red points show fake and real sources respectively.

Figure 20 shows the behavior of $w?snr$ and $w?rchi2$ in real and fake sources in the four WISE bands. The left and right columns of plots show different zoom levels of the full distribution in these parameters (left: zoomed out, right: zoomed in). For each band we show the distribution separately between the two test fields (as labeled in the upper corner of the plots). Real and fake sources are found in overlapping, but different regions of this parameter space that we use to separate the two in the *AllWISE* catalog.

Figure 21 shows the behavior of $w?nm/w?m$ versus $w?m$ in 'real' and 'fake' sources in the four *WISE* bands, where $w?nm$ is the number of profile-fit flux measurements for a source with $w?snr > 3$ and $w?m$ is the number of profile-fit flux measurements for a source. The symbol size scales with the number of objects at that set of values for the two parameters as shown in the figure legend. The left column of plots shows the behavior in the W3 test field, while the right column shows the W5 test field. For the most part in bands 1, 2 and

3, both real and fake sources have similar distributions of these parameters when plotted in this way. In band 4 a different pattern appears, with a much larger fraction of the fake sources having $w4nm/w4m < 0.2$. The contrast between real and fake source distributions is not strong enough to be used as an effective discriminant in the catalog, however.

Figure 22 shows the behavior of the profile fit ($w?mpro$) and aperture ($w?mag$) magnitudes values for 'real' and 'fake' sources in the *AllWISE* catalog in the two test fields. We plot $w?mpro - w?mag$ versus $w?mpro$, with the left column of plots showing the behavior in the W3 test field and the right column showing the W5 test field. In bands 1 and 2, a cut of $|w?mpro - w?mag| < 0.5$ would effectively remove the fake sources, while at the same time allowing through the majority of the real objects (see Table 9). A reader may validly pursue a cut based on aperture and profile fit magnitude offsets in bands 1 and 2 as an alternative to SNR vs. χ^2_ν. However, in bands 3 and 4, fake sources are so numerous and occupy such a large portion of this parameter space that no good cut to remove them and keep enough real sources can be found to compete with our $w?snr$ and $w?rchi2$-based cut in these bands.

REFERENCES

Acker, A., Marcout, J., Ochsenbein, F., Stenholm, B., & Tylenda, R. 1992, Strasbourg-ESO Catalogue of Galactic Planetary Nebulae, Parts I, II (Garching: European Southern Observatory)

Alksnis, A., Balklavs, A., Dzervitis, U., et al. 2001, VizieR Online Data Catalog, 3227, 0

Allen, L. E., Calvet, N., D'Alessio, P. et al. 2004, ApJS, 154, 363

Allen, T. S., Gutermuth, R. A., Kryukova, E., et al. 2012, ApJ, 750, 125

André, P., Men'shchikov, A., Bontemps, S., et al. 2010, A&A, 518, L102

Andrews, S. M., Wilner, D. J., Espaillat, C., et al. 2011, ApJ, 732, 42

Assef, R. J., Kochanek, C. S., Brodwin, M., et al. 2010, ApJ, 713, 970

Bressert, E., Bastian, N., Gutermuth, R. 2010, MNRAS, 409, L54

Carey, S. J., Clark, F. O., Egan, M. P., et al. 1998, ApJ, 508, 721

Carpenter, J. M. 2000, AJ, 120, 3139

Casertano, S., & Hut, P. 1985, ApJ, 298, 80

Chengalur, J. N., Lewis, B. M., Eder, J., & Terzian, Y. 1996, VizieR Online Data Catalog, 208, 1

Cieza, L. A., Schreiber, M. R., Romero, G. A., et al. 2012, ApJ, 750, 157

Cohen, M. 1993, AJ, 105, 1860

Cohen, M., Parker, Q. A., Green, A. J., et al. 2011, MNRAS, 413, 514

Cox, D. P. 2005, ARA&A, 43, 337

de Wit, W. J., Testi, L., Palla, F., & Zinnecker, H. 2005, A&A, 437, 247

Dominik, C., & Decin, G. 2003, ApJ, 598, 626

Evans, N. J., Dunham, M. M., Jørgensen, J. K., et al. 2009, ApJS, 181, 321

Fűrész, G., Hartmann, L. W., Szentgyorgyi, A. H., et al. 2006, ApJ, 648, 1090

Greene, T. P., Wilking, B. A., André, P., Young, E. T., & Lada, C. J. 1994, ApJ, 434, 614

Gutermuth, R. A., Myers, P. C., Megeath, S. T., et al. 2008, ApJ, 674, 336

Gutermuth, R. A., Megeath, S. T., Myers, P. C., et al. 2009, ApJS, 184, 18

Hartmann, L. W., Megeath, S. T., Allen, L., et al. 2005, ApJ, 629, 881

Hillwig, T. C., Gies, D. R., Bagnuolo, Jr., W. G., et al. 2006, ApJ, 639, 1069

Hopkins, P. F. 2013, MNRAS, 428, 1950

Kessler-Silacci, J. E., Hillenbrand, L. A., Blake, G. A., & Meyer, M. R. 2005, ApJ, 622, 404

Klessen, R. S., & Burkert, A. 2000, ApJS, 128, 287

Koenig, X. P., Allen, L. E., Gutermuth, R. A., et al. 2008, ApJ, 688, 1142

Koenig, X. P., Leisawitz, D. T., Benford D. J., et al. 2012, ApJ, 744, 130

Kraus, A. L., & Hillenbrand, L. A. 2008, ApJ, 686, L111

Krumholz, M. R. 2014, Phys. Rep., in press, arXiv1402.0867

Larson, R. B. 1995, MNRAS, 272, 213

Li, A., & Draine, B. T. 2001, ApJ, 554, 778

Lindqvist, M., Winnberg, A., Habing, H. J., & Matthews, H. E. 1992, A&AS, 92, 43

McClure, M. 2009, ApJ, 693, 81

Marsh, K. A., & Jarrett, T. H. 2012, PASA, 29, 269

Masiunas, L. C., Gutermuth, R. A., Pipher, J. L., et al. 2012, ApJ, 752, 127

Mathew, B., Subramaniam, A., & Bhatt, B. C. 2008, MNRAS, 388, 1879

Miszalski, B., Parker, Q. A., Acker, A., et al. 2008, MNRAS, 384, 525

Morales, F. Y., Padgett, D. L., Bryden, G., Werner, M. W., & Furlan, E. 2012, ApJ, 757, 7

Nikutta, R., Hunt-Walker, N., Nenkova, M., Ivezić, Ž., & Elitzur, M. 2014, arXiv:1405.7966

Offner, S. S. R., Hansen, C. E., & Krumholz, M. R. 2009, ApJ, 704, L124

Parker, Q. A., Acker, A., Frew, D. J., et al. 2006, MNRAS, 373, 79

Peebles, P. J. E., & Hauser, M. G. 1974, ApJS, 28, 19

Pérault, M., Omont, A., Simon, G., et al. 1996, A&A, 315, L165

Polychroni, D., Moore, T. J. T., & Allsopp, J. 2010, in ASP Conf. Ser. 424, 9th International Conference of the Hellenic Astronomical Society, ed. K. Tsinganos, D. Hatzidimitriou, & T. Matsakos (San Francisco, CA: ASP), 165

Rathborne, J. M., Jackson, J. M., & Simon, R. 2006, ApJ, 641, 389

Rebull, L. M., Padgett, D. L., McCabe, C.-E., et al. 2010, ApJS, 186, 259

Reed, B. C. 2000, AJ, 120, 314

Rivinius, T., Carciofi, A. C., & Martayan, C. 2013, A&A Rev., 21, 69

Roberts, M. S. 1957, PASP, 69, 59

Robitaille, T. P., Meade, M. R., Babler, B. L., et al. 2008, AJ, 136, 2413

Schlegel, D. J., Finkbeiner, D. P., & Davis, M. 1998, ApJ, 500, 525

Sicilia-Aguilar, A., Hartmann, L. W., Calvet, N., et al. 2006, ApJ, 638, 897

Simon, M. 1997, ApJ, 482, 81

Sjouwerman, L. O., van Langevelde, H. J., Winnberg, A., & Habing, H. J. 1998, A&AS, 128, 35

Skrutskie, M. F., Cutri, R. M., Stiening, R., et al. 2006, AJ, 131, 1163

Wainscoat, R. J., Cohen, M., Volk, K., Walker, H. J., & Schwartz, D. E. 1992, ApJS, 83, 111

Westerhout, G. 1958, Bull. Astron. Inst. Netherlands, 14, 215

Wright, E. L., Eisenhardt, P. R. M., Mainzer, A. K., et al. 2010, AJ, 140, 1868

Zinnecker, H., & Yorke, H. W. 2007, ARA&A, 45, 481

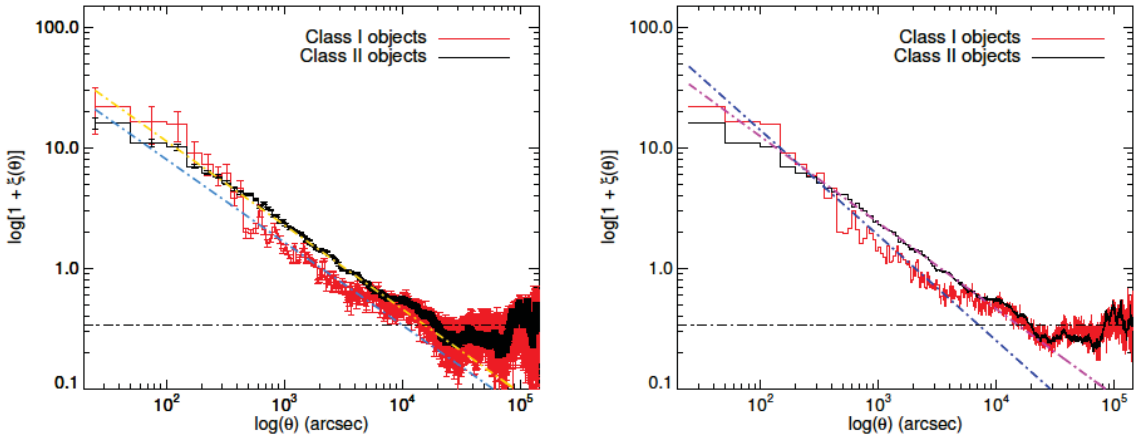

Fig. 14.— Two-point correlation function for the Class I sources (red histogram) and Class II sources (black histogram). Left panel: dot dashed lines show weighted least-squares fits to the straight-line part of the data for Class I sources (blue) and Class II sources (yellow). In the right panel we remove the error bars and overplot unweighted least squares fits to the data between 200 and 4000″ (Class I sources: blue and Class II sources: magenta). Black dot-dashed line shows level of a random distribution in this formalism.

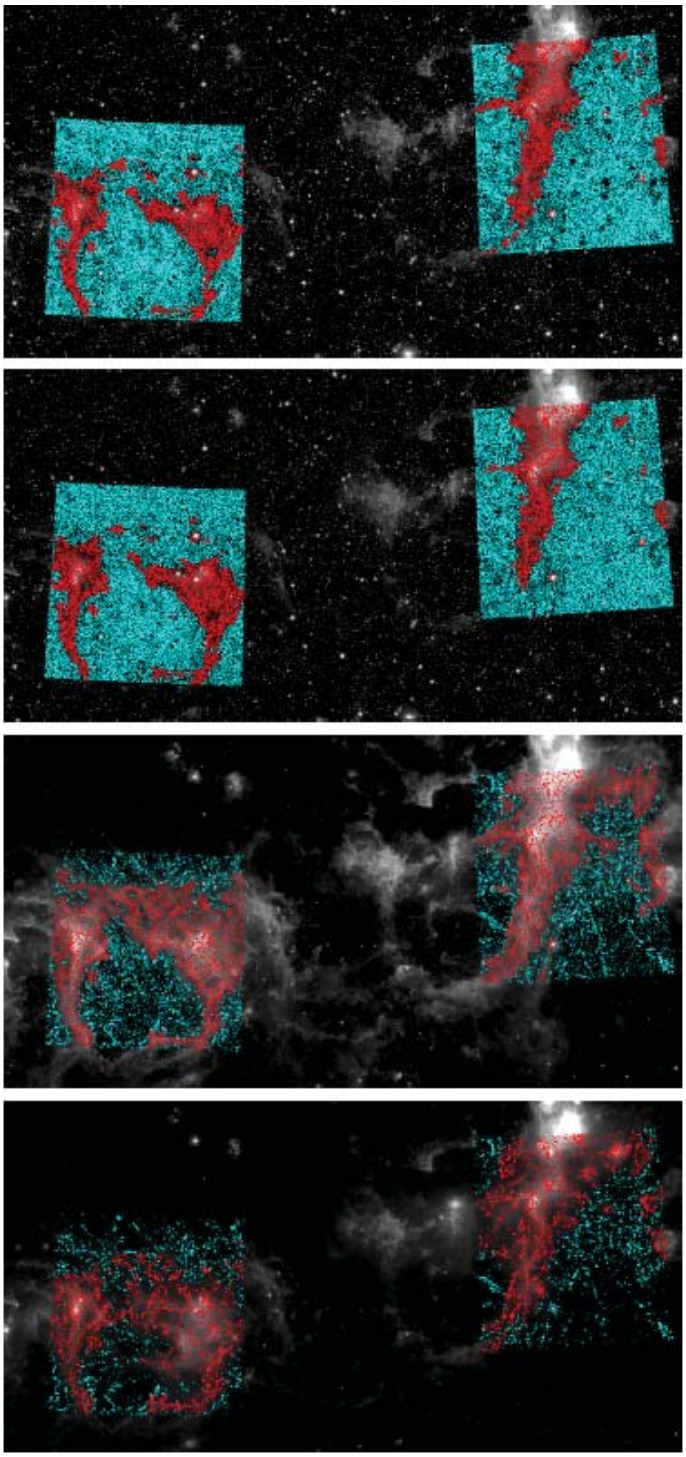

Fig. 15.— Grayscale *WISE* images in the 4 bands overlaid with sources in the two test fields in those bands, colored coded for low sky (cyan points) and high sky (red points) following the thresholds in Table 13.

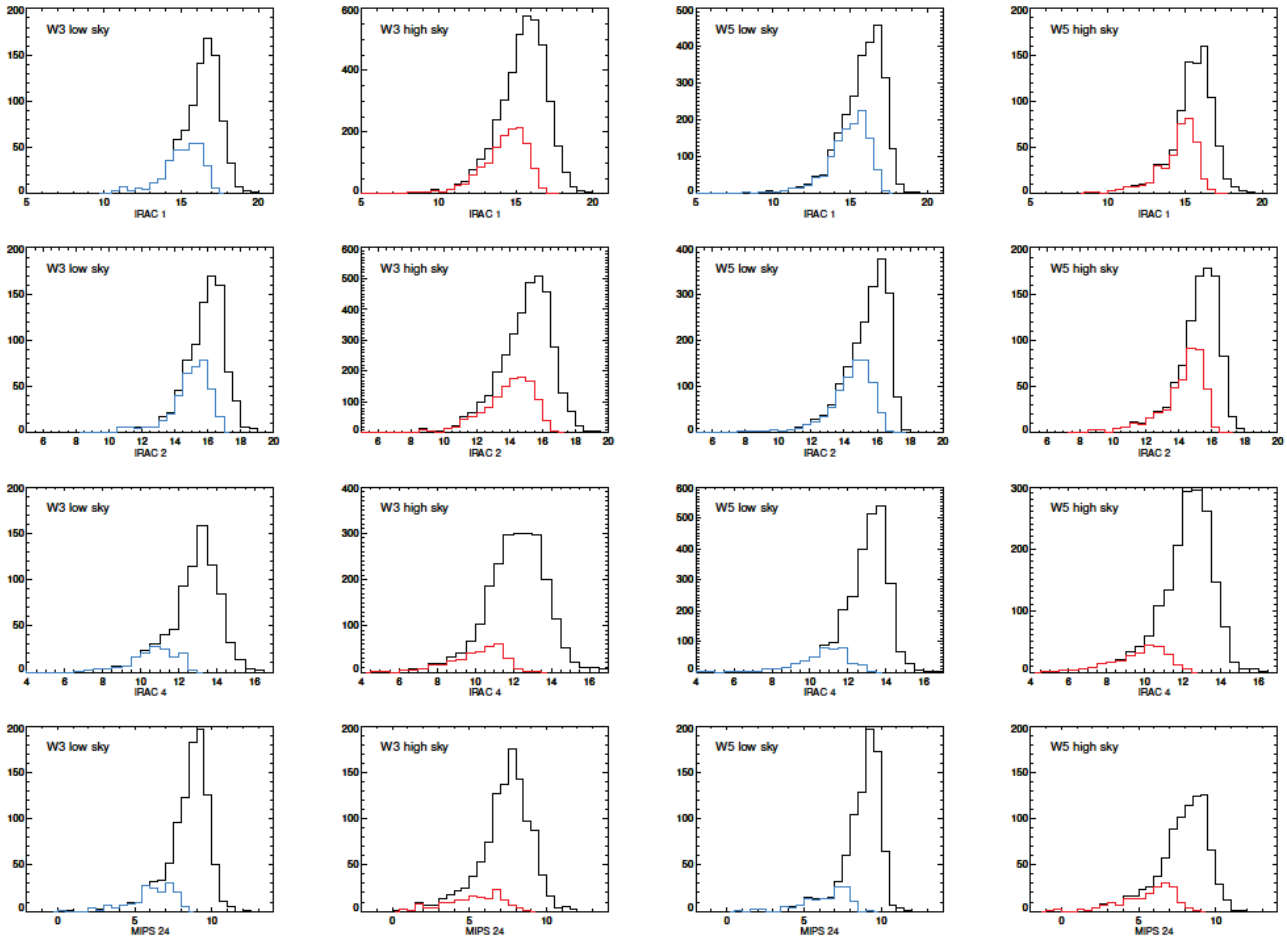

Fig. 16.— Completeness histograms for the *WISE* truth catalog source lists against the *Spitzer* catalog (black histograms), in high and low sky regions (red and blue histograms respectively) in the two test regions.

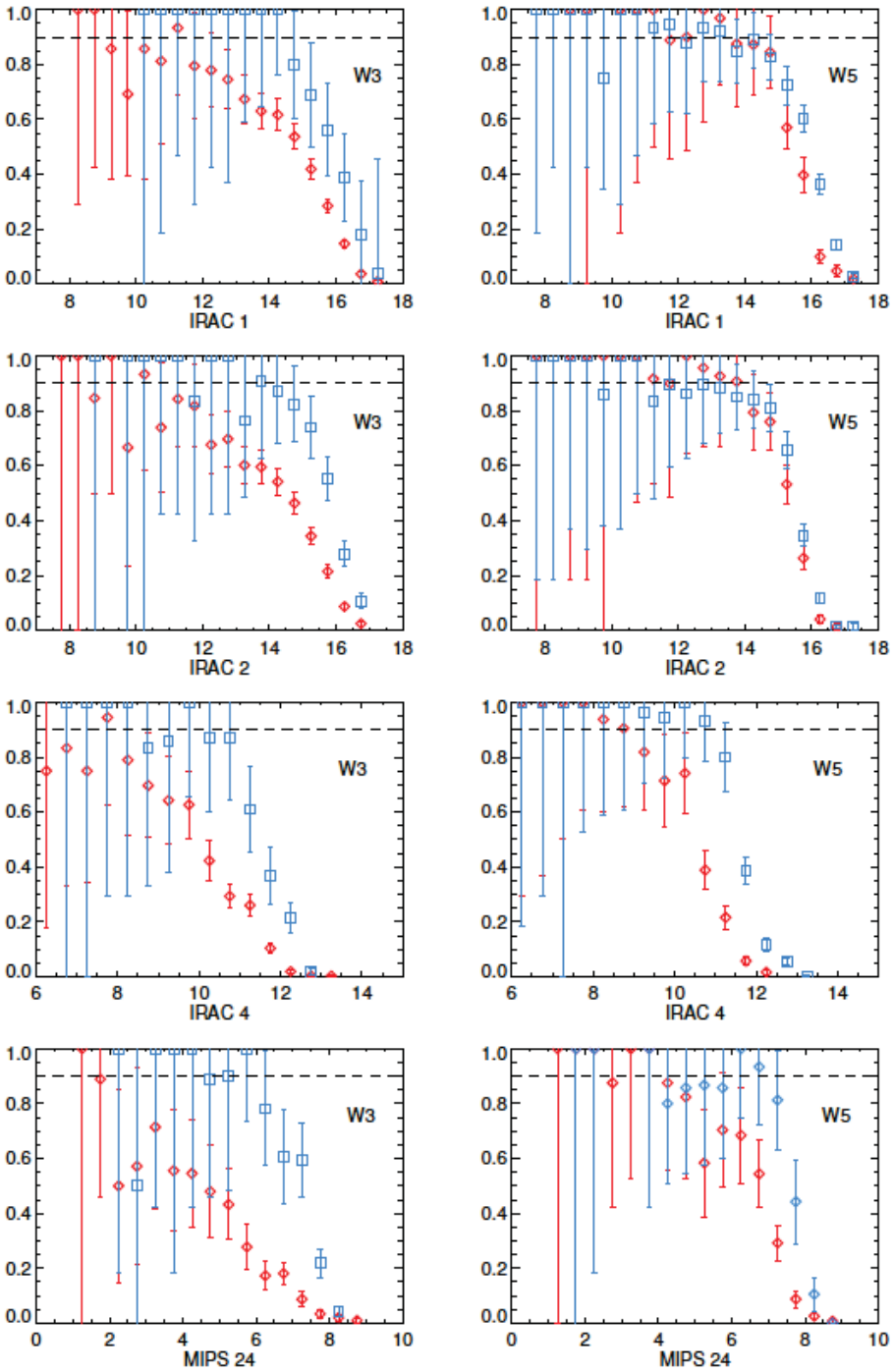

Fig. 17.— Completeness plots derived from the histograms in Figure 16 for the manual *WISE* truth catalog source lists. Red and blue points correspond to high sky and low sky regions respectively.

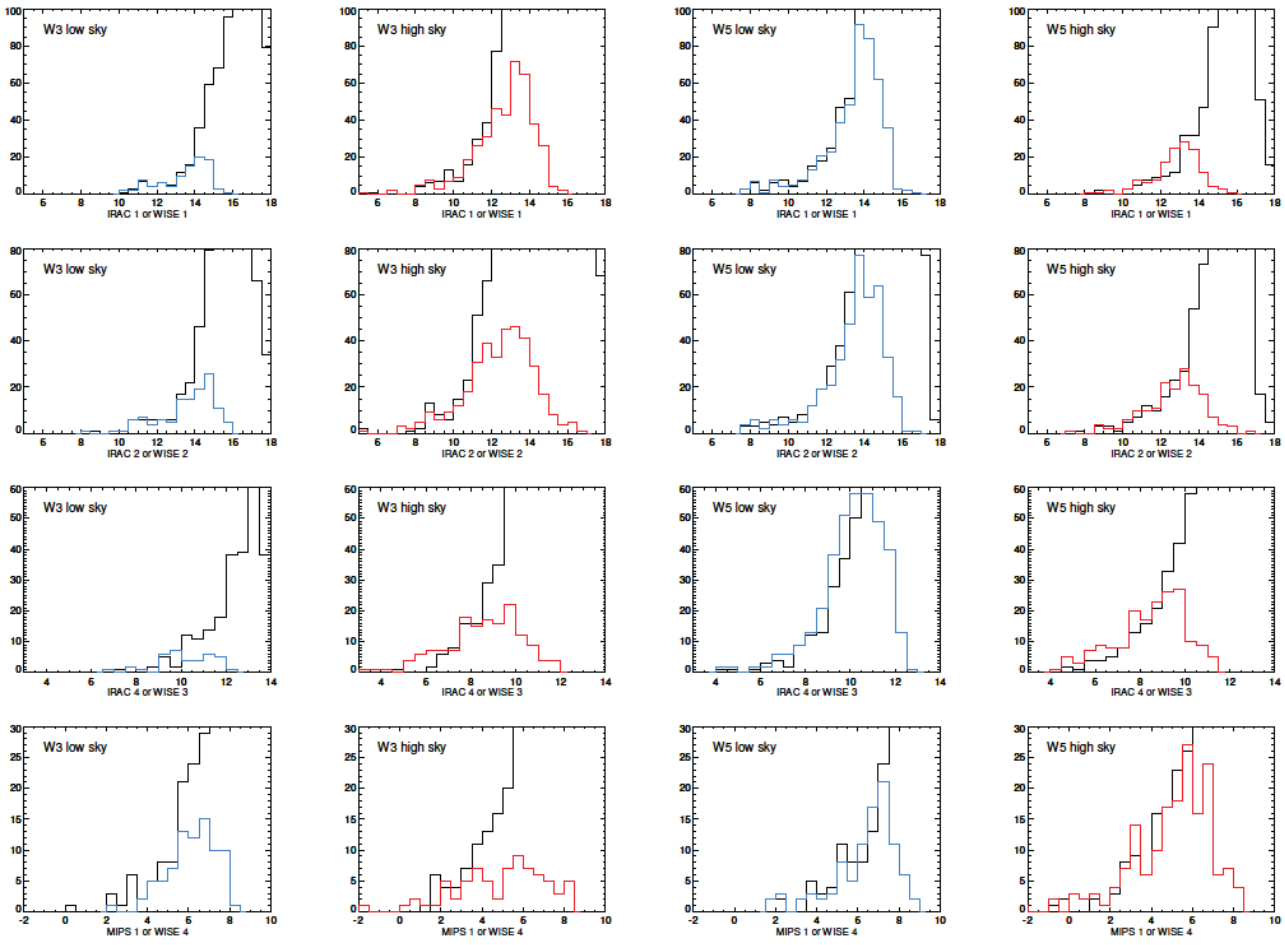

Fig. 18.— Completeness histograms for *AllWISE* retrieved truth-catalog objects compared to the *Spitzer* catalog (black histograms) in high and low sky regions (red and blue histograms respectively) in the two test regions.

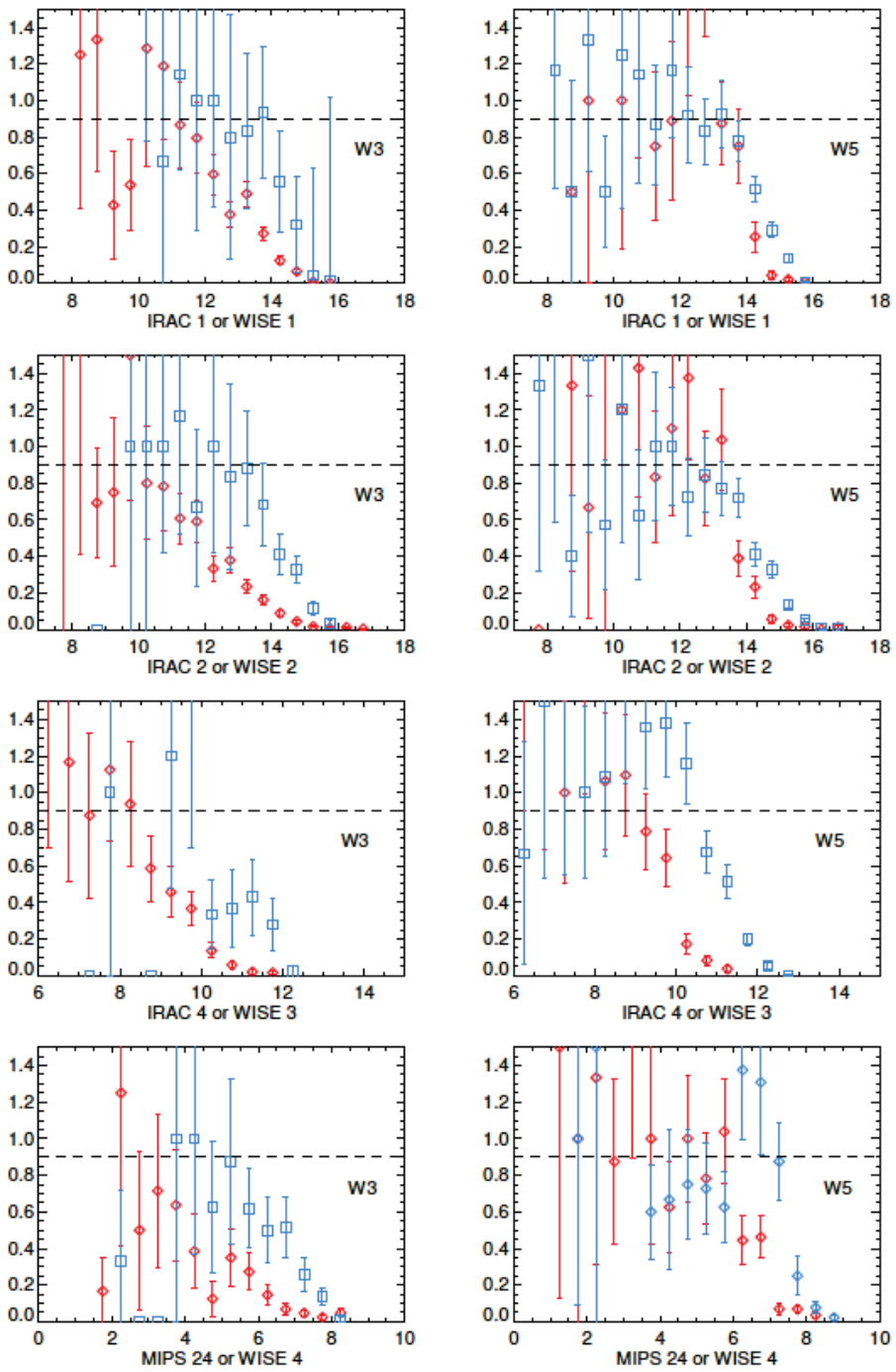

Fig. 19.— Completeness plots derived from the histograms in Figure 18 for the *AllWISE* catalog source lists. Red and blue points correspond to high and low sky regions respectively.

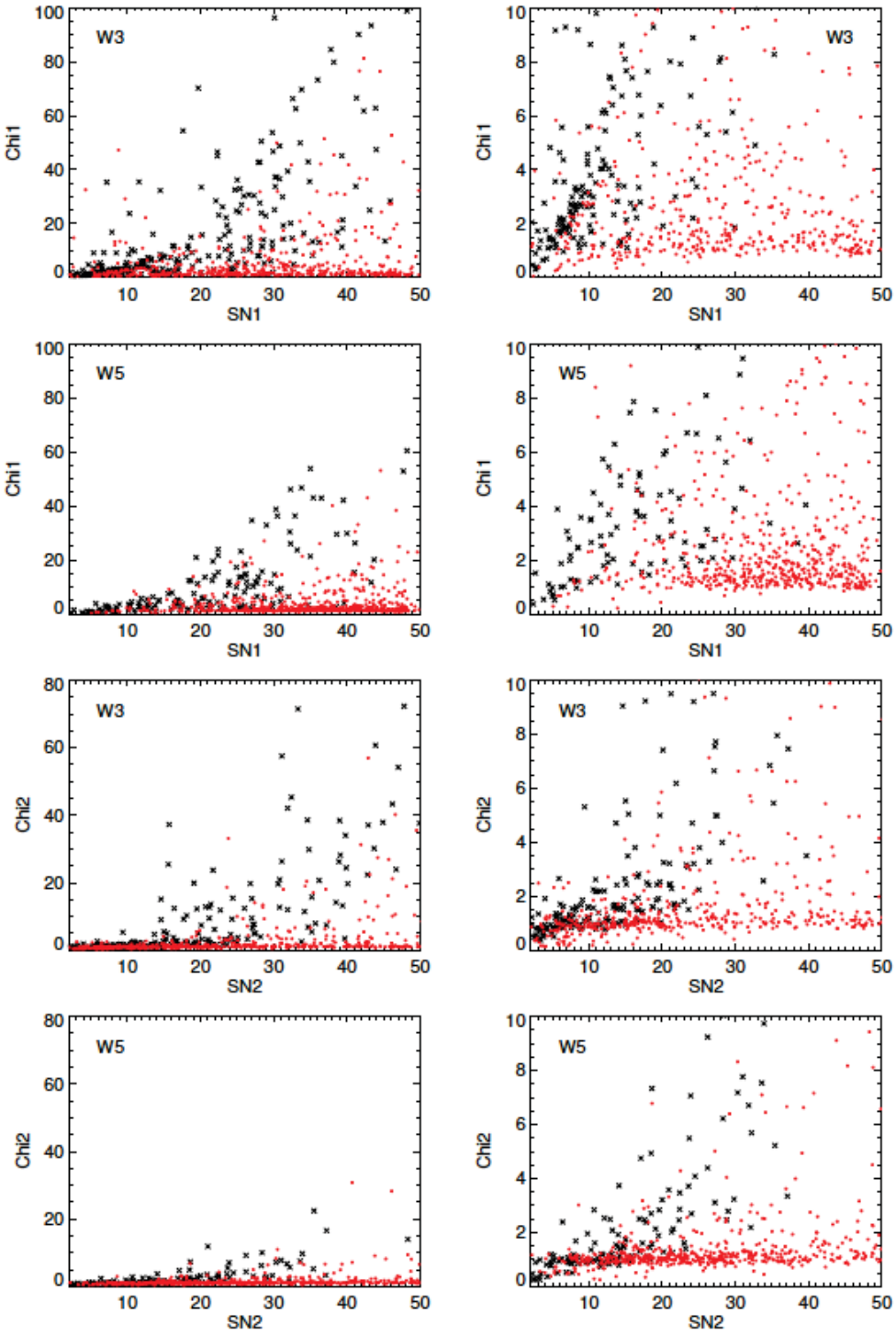

Fig. 20.— Reduced chi-squared of the profile fit photometry versus signal to noise in sources that match an object in the *WISE* truth catalogs (red points) or have no visible match (black crosses).

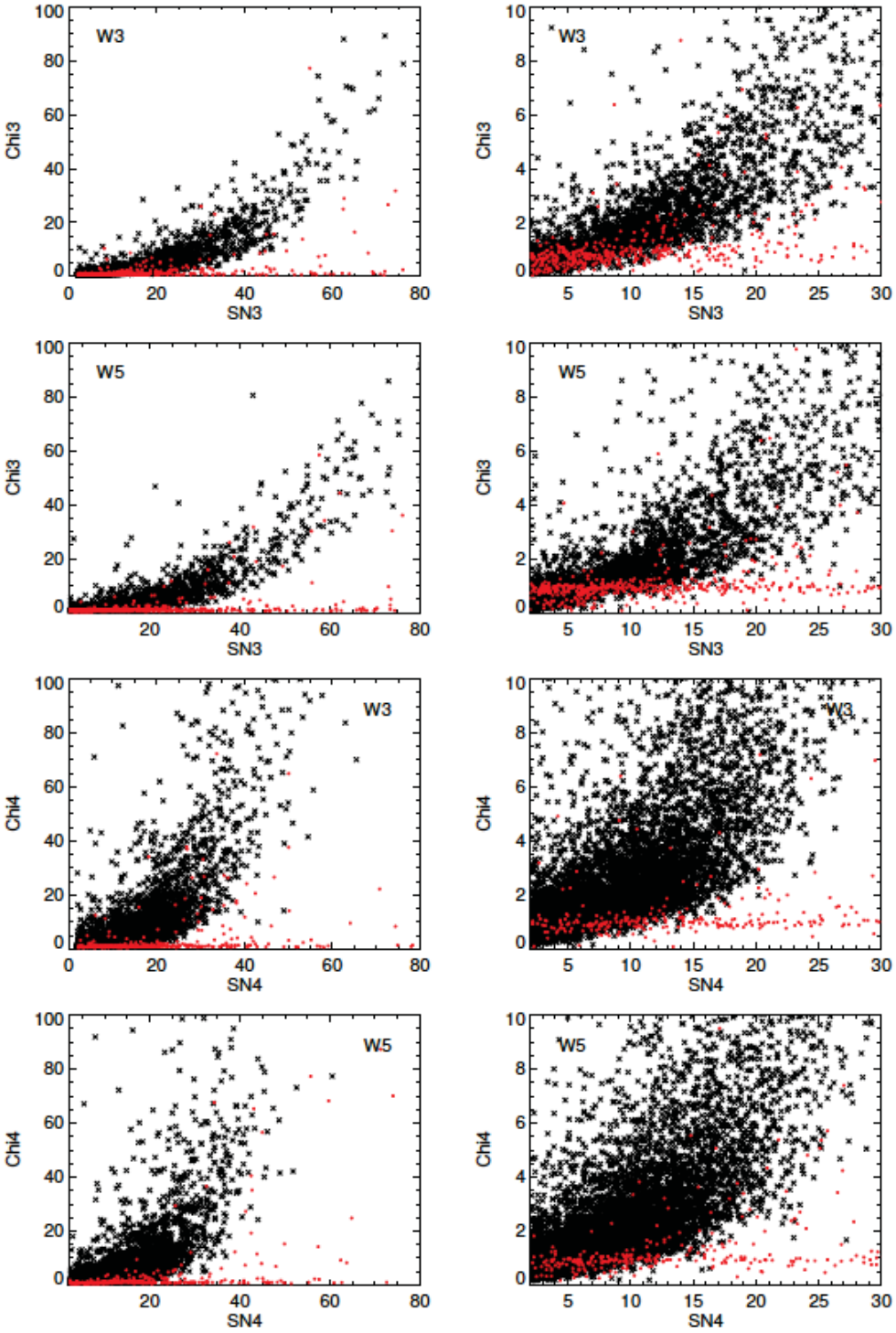
W3
Chi3
SN3
W3
Chi3
SN3
W5
Chi3
SN3
W5
Chi3
SN3
W3
Chi4
SN4
W3
Chi4
SN4
W5
Chi4
SN4
W5
Chi4
SN4

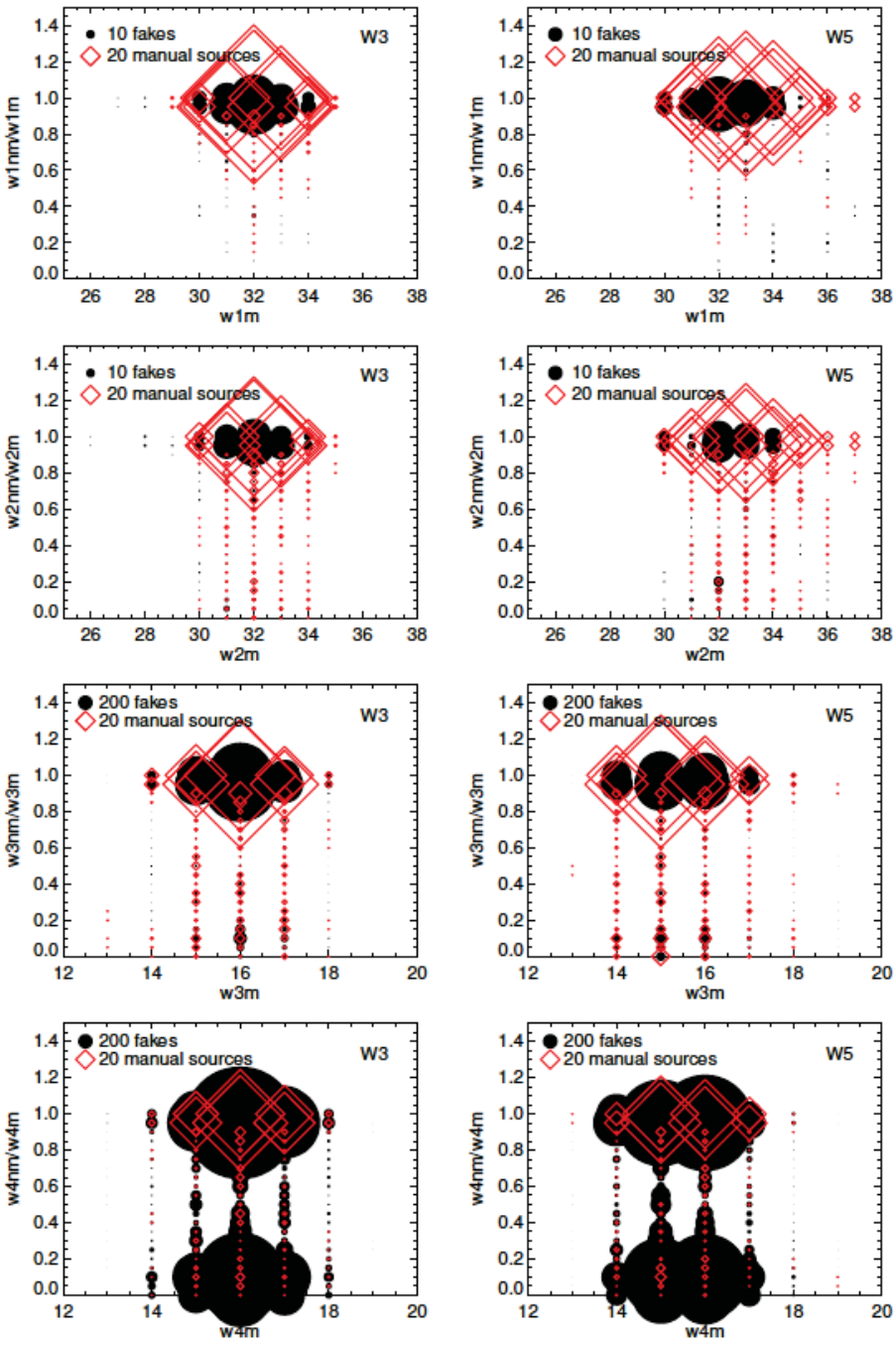

Fig. 21.— Plots showing the ratio of N detections above $w?snr = 3$ to N (all detections) versus N (all detections) for *AllWISE* sources in the two test regions. Red symbols correspond to matches to the truth catalog, black to *AllWISE* entries with no visible match in the *WISE* mosaic images. Symbol size scales with number of objects at that set of values.

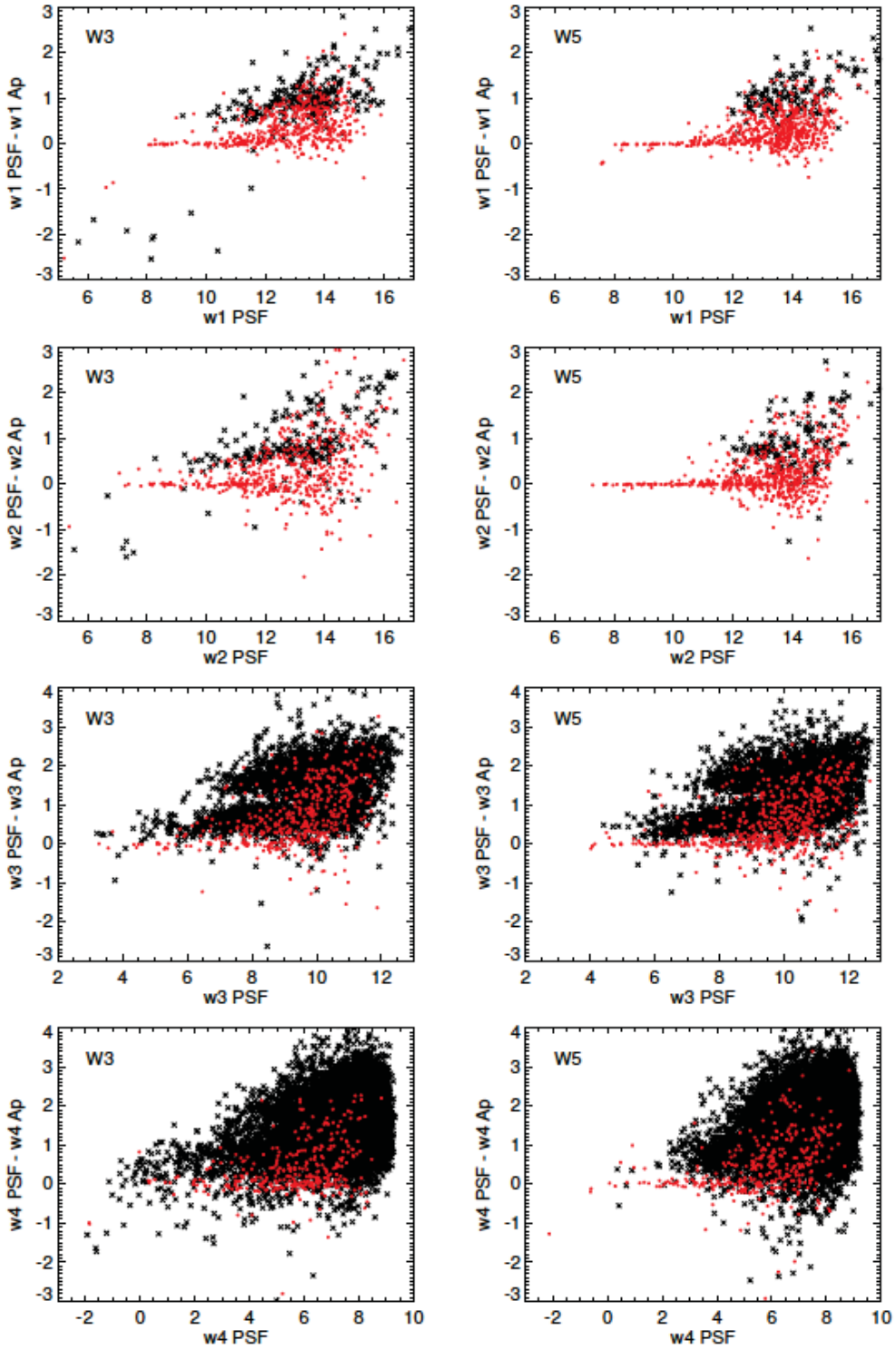

Fig. 22.— Plots showing the difference between profile fit (*w?mpro*) and aperture (*w?mag*) magnitudes in all bands in *AllWISE* sources with a match in the truth catalogs (red points) and those with no match (black points).